Inorganic Chemistry

Article

pubs.acs.org/IC

Mixed Ligand Copper(II) Complexes of *N*,*N*-Bis(benzimidazol-2-ylmethyl)amine (BBA) with Diimine Co-Ligands: Efficient Chemical Nuclease and Protease Activities and Cytotoxicity

Rangasamy Loganathan,[†] Sethu Ramakrishnan,[†] Eringathodi Suresh,[‡] Anvarbatcha Riyasdeen,[§] Mohamad Abdulkadhar Akbarsha,[∥,⊥] and Mallayan Palaniandavar*[,†,#]

[†]Centre for Bioinorganic Chemistry, School of Chemistry, Bharathidasan University, Tiruchirappalli 620 024, Tamilnadu, India

[‡]Analytical Science Discipline, Central Salt and Marine Chemical Research Institute, Bhavnagar 364 002, India

[§]Department of Animal Science, Bharathidasan University, Tiruchirappalli 620 024, Tamilnadu, India

[∥]Mahatma Gandhi-Doerenkamp Center for Alternatives to Use of Animals in Life Science Education, Bharathidasan University, Tiruchirappalli, 620024, Tamilnadu, India

Supporting Information

ABSTRACT: A series of mononuclear mixed ligand copper(II) complexes [Cu(bba)(diimine)]$(ClO_4)_2$ **1**–**4**, where bba is *N*,*N*-bis(benzimidazol-2-ylmethyl)-amine and diimine is 2,2′-bipyridine (bpy) (**1**), 1,10-phenanthroline (phen) (**2**), 5,6-dimethyl-1,10-phenanthroline (5,6-dmp) (**3**), or dipyrido[3,2-*d*:2′,3′-*f*]-quinoxaline (dpq) (**4**), have been isolated and characterized by analytical and spectral methods. The coordination geometry around copper(II) in **2** is described as square pyramidal with the two benzimidazole nitrogen atoms of the primary ligand bba and the two nitrogen atoms of phen (**2**) co-ligand constituting the equatorial plane and the amine nitrogen atom of bba occupying the apical position. In contrast, the two benzimidazole nitrogen atoms and the amine nitrogen atom of bba ligand and one of the two nitrogen atoms of 5,6-dmp constitute the equatorial plane of the trigonal bipyramidal distorted square based pyramidal (TBDSBP) coordination geometry of **3** with the other nitrogen atom of 5,6-dmp occupying the apical position. The structures of **1**–**4** have been optimized by using the density functional theory (DFT) method at the B3LYP/6-31G(d,p) level. Absorption spectral titrations with Calf Thymus (CT) DNA reveal that the intrinsic DNA binding affinity of the complexes depends upon the diimine co-ligand, dpq (**4**) > 5,6-dmp (**3**) > phen (**2**) > bpy (**1**). The DNA binding affinity of **4** is higher than **2** revealing that the π-stacking interaction of the dpq ring in between the DNA base pairs with the two bzim moieties of the bba ligand stacked along the DNA surface is more intimate than that of phen. The complex **3** is bound to DNA more strongly than **1** and **2** through strong hydrophobic interaction of the methyl groups on 5,6-positions of the phen ring in the DNA grooves. The extent of the decrease in relative emission intensities of DNA-bound ethidium bromide (EB) upon adding the complexes parallels the trend in DNA binding affinities. The large enhancement in relative viscosity of DNA upon binding to **3** and **4** supports the DNA binding modes proposed. Interestingly, the 5,6-dmp complex **3** is selective in exhibiting a positive induced CD band (ICD) upon binding to DNA suggesting that it induces a B to A conformational change. In contrast, **2** and **4** show induced CD responses indicating their involvement in strong DNA binding. Interestingly, only the dpq complex **4**, which displays the strongest DNA binding affinity and is efficient in cleaving DNA in the absence of an activator with a rate constant of 5.8 ± 0.1 h^{-1}, which is higher than the uncatalyzed rate of DNA cleavage. All the complexes exhibit oxidative DNA cleavage ability, which varies as **4** > **2** > **3** > **1** (ascorbic acid) and **3** > **2** > **4** > **1** (H_2O_2). Also, the complexes cleave the protein bovine serum albumin in the presence of H_2O_2 as an activator with the cleavage ability varying in the order **3** > **4** > **2** > **1**. The highest efficiency of **3** to cleave both DNA and protein in the presence of H_2O_2 is consistent with its strong hydrophobic interaction with the biopolymers. The IC_{50} values of **1**–**4** against cervical cancer cell lines (SiHa) are almost equal to that of cisplatin, indicating that they have the potential to act as effective anticancer drugs in a time-dependent manner. The morphological assessment data obtained by using acridine orange/ethidium bromide (AO/EB) and Hoechst 33258 staining reveal that **3** induces apoptosis much more effectively than the other complexes. Also, the alkaline single-cell gel electrophoresis study (comet assay) suggests that the same complex induces DNA fragmentation more efficiently than others.

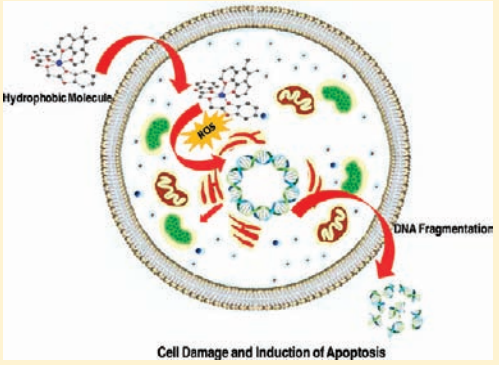

INTRODUCTION

The platinum-based drug cisplatin has been used widely and effectively in antitumor therapy for over the past three decades.

Received: August 7, 2011
Published: May 4, 2012

   dx.doi.org/10.1021/ic2017177 | *Inorg. Chem.* 2012, 51, 5512–5532

Scheme 1. Representation of Copper(II) Complexes 1−4 and the Diimine Co-Ligands

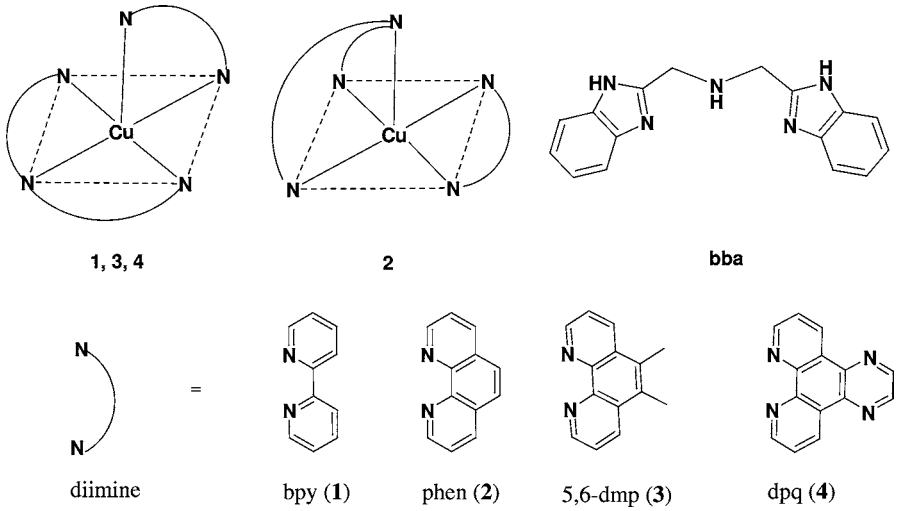

The dose of cisplatin that can be applied to patients is limited by its high toxicity, and the side effects of cisplatin therapy include damage to the kidney (nephrotoxicity), hearing (ototoxicity), peripheral neuropathy and neurotoxicity, nausea, and vomiting.[1] Copper[2−5] and ruthenium[6−12] complexes are regarded as promising alternatives to platinum complexes as anticancer drugs. Copper, an essential element for most aerobic organisms, is employed as a structural and catalytic cofactor, and consequently it is involved in many biological pathways.[15−18] Also, serum copper levels correlate with tumor incidence, tumor weight, malignant progression, and recurrence in a variety of human cancers: Hodgkin's lymphoma, sarcoma, leukemia, and cancer of the cervix, breast, liver, and lung[19−22] as well as brain tumors,[23,24] supporting the idea that copper could be used as a potential tumor-specific target. Several copper complexes[2−5,13,14,23−29] have been now proposed as potential anticancer substances and cancer inhibiting agents, as they demonstrate remarkable anticancer activity and show general toxicity lower than platinum compounds.

Very recently, mixed ligand copper(II) complexes are found to exhibit prominent anticancer activity by inducing apoptosis, and interestingly they are found to strongly bind and cleave DNA.[4,5,30−32] In general, redox-active agents that damage DNA in vitro are thought to exhibit apoptotic activities in live cells by inducing oxidative stress and/or DNA damage. Among various forms of DNA damage, the double-strand DNA cleavage is considered to be the most dangerous form.[33] Even a single double-strand cleavage is sufficient to kill a cell due to the intrinsic difficulty in repairing a severed DNA molecule. Double-strand breaks (dsb's) are thought to be more significant biologically than are single strand breaks (ssb's) as sources of cell lethality, because they are apparently less readily repaired by DNA repair mechanisms.[33] The most promising antitumor agents enediynes[34] and bleomycins[35] are known to cause both single-strand and double-strand breaks in duplex DNA. We have very recently found that the prominent anticancer activities of certain mixed ligand Cu(II) complexes[31] are consistent with the ability of the complexes to affect double-stand DNA cleavage. Sigman and his co-worker have shown that copper complexes of 1,10-phenanthroline (phen) act as effective chemical nucleases with a high preference for double-stranded DNA in the presence of molecular oxygen and a reducing agent.[36] In fact, many other copper(II) complexes[37−41] have been shown to be capable of mediating non-random double-strand cleavage of plasmid DNA. However, no attempt has been made to study their anticancer activities and relate them to their ability to cleave double-strand DNA cleavage.

In this work, we have isolated a series of mixed ligand copper(II) complexes of the type $[Cu(bba)(diimine)](ClO_4)_2$, where bba is *N*,*N*′-bis(benzimidazol-2-ylmethyl)amine and diimine is 2,2′-bipyridine (bpy) (**1**) or 1,10-phenanthroline (phen) (**2**) or 5,6-dimethyl-1,10-phenanthroline (5,6-dmp) (**3**) or and dipyrido[3,2-*d*:2′,3′-*f*]quinoxaline (dpq) (**4**) and study their DNA binding and cleaving propensities. The tridentate primary ligand bba would be expected to tune the electronic properties of copper(II) complexes. Thus, the weakly π-accepting benzimidazole (bzim) nitrogen donors have been shown to raise the Cu^{II}/Cu^{I} redox potentials significantly by stabilizing the lower oxidation state[42] of copper and bzim moieties may have the potential to enhance DNA binding through hydrophobic interaction with DNA. Metal complexes containing bzim ligand moieties form an important class of biologically active compounds that can efficiently hydrolyze a phospho-diester bond[43] and cleave supercoiled pBR322 DNA.[43] Also, ligands incorporating bzim moieties selectively interact with a specific nucleotide sequence and bind to the minor groove of A−T tract duplex DNA[44,45] and a bzim unit provides a conformationally stable and appropriate platform on which to build further DNA sequence recognition.[46] The design of a molecule, which can affect double-strand DNA cleavage activities, must include a reactivatable metal center like copper and also recognition elements that bind to duplex DNA and at nicked sites as well.

The diimine co-ligands have been chosen to function as DNA recognition elements as they play a pivotal role in the mechanism underlying induction of cell death by mixed ligand complexes of Cu(II),[32,47] Ru(II),[48] Fe(II),[49] Ni(II),[49] and Co(III).[49] Also, the hydrophobic methyl groups of 5,6-dmp co-ligand would provide a hydrophobic recognition element[84] to interact with DNA bases. The DNA-binding propensities of the present complexes have been explored to understand the chemical principles underlying site-specific DNA recognition in biological systems. Also, the complexes are remarkable in bringing out efficient oxidative as well as hydrolytic cleavage of DNA in the absence of a reductant.

dx.doi.org/10.1021/ic2017177 | *Inorg. Chem.* 2012, 51, 5512−5532

When a cytotoxic metal-containing compound is administered intravenously, it may interact with macromolecular blood components like proteins, which can then be taken up by and get accumulated in tumor tissue. So, we have also investigated the protein binding and cleavage of the complexes using a serum protein like bovine serum albumin (BSA), which may perform a transport function for the drug. Also, such interactions would determine the overall drug distribution and excretion and differences in efficacy, activity, and toxicity.[51,52] Cervical cancer is the second most common cause of cancer-related death among women worldwide[53] and the currently used drug cisplatin is limited by its side effects. Therefore we chose to screen the cytotoxicity of the DNA-cleaving copper(II) complexes toward SiHa human cervical cancer cell lines. The complexes exhibit IC_{50} values that are almost equal to cisplatin for the same cell lines, indicating that they are promising drugs for cancer treatment. Also, it is remarkable that the complex with 5,6-dmp co-ligand kills the cancer cell lines through apoptosis more efficiently than that with dpq as co-ligand. An important realization from this work is the very remarkable correlation between the DNA double-strand cleavage efficiency and cytotoxicity of complexes.

EXPERIMENTAL SECTION

Materials and Reagents. Copper(II) perchlorate hexahydrate (Aldrich), 1,10-phenanthroline, 2,2′-bipyridine (Loba), 5,6-dimethyl-1,10-phenanthroline (Aldrich), CT DNA (highly polymerized stored at 4 °C), distamycin-A, superoxide dismutase (SOD), catalase (Sigma, stored at −20 °C), pUC19 supercoiled plasmid DNA, agarose, BSA and protein markers (Genei, Bangalore, India), and Tris-(hydroxymethyl)aminomethane (Merck) were used as received. Ultrapure Milli Q water (18.3 $\mu\Omega$) was used for all the experiments. The commercial solvents were distilled and then used for the preparation of ligands and complexes.

Synthesis of Ligands. The ligands *N*,*N*′-bis(benzimidazol-2-ylmethyl)amine (bba) and dipyridoquinoxaline (dpq) were prepared according to the reported procedures[46,54] and purified by using Teledyne ISCO CombiFlash chromatograph using prepacked RediSep column.

Synthesis of Copper(II) Complexes. CAUTION! During handling of the perchlorate salts of metal complexes with organic ligands care should be taken because of the possibility of explosion.

[Cu(bba)Cl$_2$]. The complex [Cu(bba)Cl$_2$] was synthesized according to the reported procedure.[46]

[Cu(bba)(bpy)](ClO$_4$)$_2$ (1). The complex **1** was prepared by adding a solution of copper(II) perchlorate hexahydrate (0.370 g, 1 mmol) in methanol/water (5:1 v/v) to a methanolic solution of 2,2′-bipyridine (0.156 g, 1 mmol) and *N*,*N*′-bis(benzimidazol-2-ylmethyl)amine (0.277 g, 1 mmol) and then stirring the solution for 1 h. The blue precipitate obtained was collected by suction filtration, washed with small amounts of cold methanol and diethyl ether, and then dried in a vacuum. Anal. Calc. for $C_{26}H_{23}Cl_2CuN_7O_8$. C, 44.87; H, 3.33; N, 14.09. Found: C, 44.81; H, 3.39; N, 14.16%. Λ_M /Ω^{-1} cm^2 mol^{-1}: 218. λ_{max}/nm, 2% DMF - 5 mM Tris-HCl/50 mM NaCl buffer solution (ε_{max}/dm^3 mol^{-1} cm^{-1}): 224 (7430), 277 (11300), 635 (58). ESI−MS (MeCN) displays a peak at *m*/*z* 248.13 [Cu(bba)(bpy)]$^{2+}$.

[Cu(bba)(phen)](ClO$_4$)$_2$·CH$_3$OH (2). The complex **2** was prepared by adopting the procedure used for obtaining **1** by using phen instead of bpy. The blue-colored crystals of **2** suitable for X-ray diffraction studies were obtained by dissolving the complex in acetonitrile and allowing it to crystallize. Anal. Calc. for $C_{28}H_{23}Cl_2CuN_7O_8$. C, 46.71; H, 3.22; N, 13.62. Found: C, 46.86; H, 3.20; N, 13.73%. Λ_M /Ω^{-1} cm^2 mol^{-1}: 220. λ_{max}/nm 2% DMF - 5 mM Tris-HCl/50 mM NaCl buffer solution (ε_{max}/dm^3 mol^{-1} cm^{-1}): 230 (10935), 270 (35500), 638 (66). ESI−MS (MeCN) displays a peak at *m*/*z* 260.20 [Cu(bba)(phen)]$^{2+}$.

[Cu(bba)(5,6-dmp)](ClO$_4$)$_2$ (3). The complex **3** was prepared by using the procedure employed for obtaining **1** by using 5,6-dmp instead of bpy. Blue-colored crystals of **3** suitable for X-ray diffraction studies were obtained by dissolving **3** in acetonitrile and allowing it to crystallize. Anal. Calc. for $C_{30}H_{27}Cl_2CuN_7O_8$. C, 48.17; H, 3.64; N, 13.11. Found: C, 48.24; H, 3.68; N, 13.19%. Λ_M /Ω^{-1} cm^2 mol^{-1}: 219. λ_{max}/nm 2% DMF - 5 mM Tris-HCl/50 mM NaCl buffer solution (ε_{max}/dm^3 mol^{-1} cm^{-1}): 230 (9930), 278 (35400), 639 (48). ESI−MS (MeCN) displays a peak at *m*/*z* 274.27 [Cu(bba)(5,6-dmp)]$^{2+}$.

[Cu(bba)(dpq)](ClO$_4$)$_2$ (4). The complex **4** was prepared as a blue-colored solid by employing the procedure used for isolating **1** by using dpq instead of bpy. Anal. Calc. For $C_{30}H_{23}Cl_2CuN_9O_8$ C, 46.67; H, 3.00; N, 16.58. Found: C, 46.80; H, 3.07; N, 16.66%. Λ_M /Ω^{-1} cm^2 mol^{-1}: 222. λ_{max}/nm 2% DMF - 5 mM Tris-HCl/50 mM NaCl buffer solution (ε_{max}/dm^3 mol^{-1} cm^{-1}): 258 (52360), 294 (26900), 680 (52). ESI−MS (MeCN) displays a peak at *m*/*z* 286.55 [Cu(bba)(dpq)]$^{2+}$.

EXPERIMENTAL METHODS

Microanalysis (C, H, and N) were carried out with a Vario EL elemental analyzer. A Micro mass Quattro II triple quadrupole mass spectrometer was employed for ESI−MS analysis. UV−vis spectroscopy was recorded on a Shimadzu UV−vis spectrophotometer using cuvettes of 1 cm path length. Emission intensity measurements were carried out by using a Jasco F 6500 spectrofluorimeter. Electron paramagnetic resonance (EPR) spectra for polycrystalline copper(II) complexes were obtained on a JEOL FA200 ESR spectrometer at room temperature. EPR spectra of the complexes in double distilled acetonitrile at liquid nitrogen temperature (77 K) were recorded on a JEOL JES-TE100 ESR spectrometer operating at X-band frequencies and having a 100 kHz field. 2,2′-Diphenyl-l-picrylhydrazyl (DPPH) was used as the field marker. The viscosity measurements were carried out on a Schott Gerate AVS 310 automated viscometer thermostatted at 25 °C in a constant temperature bath. Circular dichroic spectra of DNA were obtained by using JASCO J-716 spectropolarimeter equipped with a Peltier temperature control device. Cyclic voltammetry and differential pulse voltammetry on a platinum sphere electrode were performed at 25.0 ± 0.2 °C. The temperature of the electrochemical cell was maintained using a cryocirculator (HAAKE D8-G). Voltammograms were generated with the use of an EG&G PAR model 273 potentiostat. A Pentium IV computer along with EG&G M270 software was employed to control the experiments and to acquire the data. A three-electrode system consisting of a platinum sphere (0.29 cm^2), a platinum auxiliary electrode, and a reference electrode were used. The reference electrode for nonaqueous solution was Ag(s)/Ag$^+$, which consists of Ag wire immersed in a solution of $AgNO_3$ (0.01 M) and tetra-*n*-butylammonium perchlorate (0.1 M) in acetonitrile placed in a tube fitted with a vycor plug using a sleeve.[55] The cyclic voltammograms (CV) and differential pulse voltammograms (DPV) of **1**−**4** were obtained in methanol solutions with tetra-*n*-butylammonium perchlorate as the supporting electrolyte at ambient temperatures under N_2. Redox potentials were measured relative to Ag/Ag$^+$ reference electrode. All the complexes are electroactive with respect to the metal center in the potential range ±1.0 V. The redox potential ($E_{1/2}$) was calculated from the anodic (E_{pa}) and cathodic (E_{pc}) peak potentials of CV traces as (E_{pa} + E_{pc})/2 and also from the peak potential (E_{pa}) of DPV response as E_p + ΔE/2 (ΔE is the pulse height).

Solutions of DNA in the buffer 2% DMF - 5 mM Tris-HCl/50 mM NaCl buffer (pH = 7.2) in water gave the ratio of UV absorbance at 260 and 280 nm, A_{260}/A_{280}, of 1.9, indicating that the DNA was sufficiently free of protein.[56] Concentrated stock solutions of DNA were prepared in a buffer and sonicated for 25 cycles, where each cycle consisted of 30 s with 1 min intervals. The concentration of DNA in nucleotide phosphate (NP) was determined by UV absorbance at 260 nm after 1:100 dilutions by taking the extinction coefficient, ε_{260} as 6600 M^{-1} cm^{-1}. Stock solutions of DNA were stored at 4 °C and used after no more than 4 days. Supercoiled plasmid pUC19 DNA was stored at −20 °C, and the concentration of DNA in base pairs was determined by UV absorbance at 260 nm after appropriate dilutions taking ε_{260} as 13 100 M^{-1} cm^{-1}. Concentrated stock solutions of copper complexes were prepared by dissolving calculated amounts of

dx.doi.org/10.1021/ic2017177 | Inorg. Chem. 2012, 51, 5512−5532

the complexes in respective amounts of solvent and diluted suitably with the corresponding buffer to the required concentrations for all experiments. MALDI-TOF mass spectra were recorded on a Bruker Daltonics Ultraflex MALDI-TOF instrument.

X-ray Crystallography. The crystals of **2** and **3** of suitable size were selected from the mother liquor and then mounted on the tip of a glass fiber and cemented using epoxy resin. Intensity data for both the crystals were collected using Mo−Kα (k = 0.71073) radiation on a Bruker SMART Apex diffractometer equipped with a CCD area detector at 100 K for **2** and at 293 K for **3**, respectively. The SMART program[57] was used for collecting frames of data, indexing the reflections, and determining the lattice parameters. The data integration and reduction were processed with SAINT[58] software. An empirical absorption correction was applied to the collected reflections with SADABS.[59] The structures were solved by direct methods using SHELXS[60] and were refined on F^2 by the full-matrix least-squares technique using the SHELXL-97[60] program package. All the non-hydrogen atoms in both the compounds were refined anisotropically until convergence is reached. Hydrogen atoms attached to the ligand moieties were stereochemically fixed. The crystallographic data and details of data collection for **2** and **3** are given in Table 3. Even though the data for **2** were collected at 100 K, some oxygen atoms of perchlorate anion show a higher temperature factor. The data for **3** were collected at room temperature and here also the lattice water and diethylether molecules show higher temperature factors, which is reflected as alerts in the checkcif report. Even though some of the atoms in the solvent molecules present in the lattice and the perchlorate anions show a little higher temperature factors for the data collected at room temperature for **3**, the cationic part of the complex is refined well and shows no discrepancy in the temperature factor.

Computational Studies. The density functional theory (DFT) calculations were carried out with the Gaussian03 program package[61] using the hybrid density functional theory (B3LYP) method. The 6-31G* basis set was used to describe C, N, and hydrogen atoms. The Cu atom was described using the LANL2DZ basis set. The full geometry optimizations were carried out for the complexes **1**−**4** and vibrational frequency calculations have been performed on these optimized structures to ensure the stationary point and no negative frequencies were found.

DNA Binding and DNA Cleavage Experiments. Concentrated stock solutions of metal complexes were prepared by dissolving them in a 2% DMF - 5 mM Tris-HCl/50 mM NaCl buffer solution (0.5 mL of DMF in 5 mL of buffer) at pH 7.2 and diluting them suitably with the corresponding buffer to required concentrations for all the experiments. For absorption and emission spectral experiments, the DNA solutions were pretreated with the solutions of metal complexes to ensure no change in the metal complex concentrations. Absorption spectral titration experiments were performed by maintaining a constant concentration of the complex and varying the nucleic acid concentration. This was achieved by dissolving an appropriate amount of the complex and DNA stock solutions while maintaining the total volume constant (1 mL). This results in a series of solutions with varying concentrations of DNA but with a constant concentration of the complex. The absorbance (A) was recorded after successive additions of CT DNA.

The ethidium bromide (EB) displacement assay was used to determine the apparent DNA binding constants (K_{app}) of the complexes. The emission intensity of EB was used as a spectral probe, as it is known to show reduced emission intensity in buffer solution because of solvent quenching, and an enhancement of the emission intensity is observed when EB intercalatively binds to CT DNA. The competitive binding of complexes **1**−**4** to CT DNA could lead to the displacement of the EB, exposing it for solvent quenching of the emission. The DNA binding affinities of the complexes were determined from the extent of reduction of the EB emission intensity.

For viscosity measurements, CT DNA concentration was kept constant (200 μM in NP) and the concentration of copper(II) complexes varied ($1/R$ = [Cu]/[DNA] = 0.0−0.50). The flow times were noted from the digital timer attached with the viscometer. Data are presented as η/η_0 vs $1/R$, where η is the relative viscosity of DNA in the presence of the complex and η_0 is the relative viscosity of DNA alone. Relative viscosity values were calculated from the observed flow time of the DNA solution (t) corrected for the flow time of the buffer alone (t_0), using the expression $\eta_0 = (t - t_0)/t_0$.

Circular dichroic spectra were obtained using 1 or 0.2 cm path length quartz cell. Each CD spectrum was collected after averaging over at least four accumulations using a scan speed of 100 nm min^{-1} and a 1 s response time. Machine plus cuvette baselines were subtracted and the resultant spectrum zeroed outside the absorption bands.

The interaction of complexes with supercoiled pUC19 DNA was monitored using agarose gel electrophoresis. In reactions using supercoiled pUC19 DNA, the plasmid DNA (SC form, 40 μM) in 2% DMF - 5 mM Tris-HCl/50 mM NaCl buffer solution at pH 7.2 was treated with copper complexes in the same buffer. In each experiment supercoiled pUC19 DNA was treated with different concentrations of complexes and also the cleavage of plasmid DNA in the absence and presence of the activating agent ascorbic acid or H_2O_2 was monitored using agarose gel electrophoresis. The samples were then incubated for 1 h at 37 °C and analyzed for the cleaved products using gel electrophoresis as discussed below. A loading buffer containing 22% bromophenol blue, 0.22% xylene cyanol, and 30% glycerol (3 μL) was added and electrophoresis was performed at 60 V for 5 h in Tris−acetate−EDTA (TAE) buffer (40 mM Tris base, 20 mM acetic acid, 1 mM EDTA) using 1% agarose gel containing 1.0 μg mL^{-1} EB. The gels were viewed in a Gel doc system and photographed using a CCD camera (Alpha Innotech Corporation). The intensities of supercoiled DNA were corrected by a factor of 1.47 as a result of the lower staining capacity of ethidium bromide.[62] The cleavage efficiency was measured by determining the ability of complexes to convert the supercoiled DNA (SC) to nicked circular form (NC) and linear form (LC). In order to identify the reactive oxygen species (ROS) involved in the cleavage reaction the radical scavengers such as hydroxyl radical (DMSO, 6 μL), singlet oxygen (NaN_3, 100 μM), superoxide (SOD, 4 unit), and H_2O_2 (catalase, 6 units) were introduced.

Investigation of Linearization of DNA. Double-stranded DNA cleavage chemistry was studied further by quantification of forms III and II. The formation of single-strand breaks (ssb) and double-strand breaks (dsb) was quantified by gel electrophoresis on plasmid DNA, and the average numbers of ssb's (n_1) and dsb's (n_2) per molecule were quantitated using a standard model, which assumes a Poisson distribution of cleavage sites.[43,63,64]

The fraction of linear DNA after scission chemistry, f(III), is related to the number (n_2) of double-stranded breaks per molecule given by the first term of a Poisson distribution (eq 1).[43,63]

$$f(\mathrm{III}) = n_2 \exp(-n_2) \quad (1)$$

The sum of single-stranded (n_1) and double-stranded (n_2) breaks per molecule ($n_1 + n_2$) was determined from the fraction f(I) of supercoiled DNA remaining after treatment with the copper(II) complexes.[43,63]

$$f(\mathrm{I}) = \exp[-(n_1 + n_2)] \quad (2)$$

The Freifelder-Trumbo relation is $n_2 = n_1^2(2h + 1)/4L$, where h is the maximum separation in base pairs between two cuts on complementary strands that produce a linear DNA molecule (16) and L is the number of phosphoester bonds per DNA strand in the pUC19 DNA plasmid (L) (2686).[64] The Freifelder-Trumbo relation (eq 2) shows that the number of double-stranded breaks expected from coincidences of random single-stranded breaks is less than 0.01 per molecule, that is, $n_1/n_2 > 120$.[64] Consequently, from comparison of the ratio of n_1 and n_2 (n_1/n_2) relative to 120, one can determine if the linearization of DNA results from random or nonrandom cleavage. In these studies, both n_1 and n_2 were calculated by using eqs 1 and 2.

Tryptophan Fluorescence Quenching. Quenching of the fluorescence emission of tryptophan residues of BSA[65] was done using complexes **1**−**4** as quenchers. To solutions of BSA in phosphate buffer at pH 7.0, increments of the quencher were added, and the emission

dx.doi.org/10.1021/ic2017177 | Inorg. Chem. 2012, 51, 5512−5532

signals at 344 nm (excitation wavelength at 295 nm) were recorded after each addition of the quencher. The I_0/I vs [complex] plot as constructed using the corrected fluorescence data taking into account the effect of dilution.

Protein Cleavage Studies. Protein cleavage experiments involve incubation of BSA with **1**−**4** in 2% DMF: 5 mM Tris-HCl/50 mM NaCl buffer at pH 7.1 for 3 h at 50 °C. At the end of the incubation period, an aliquot was mixed with a loading buffer two times (100 mM Tris-HCl; pH 6.8; 7% SDS, 20% glycerol, 2% β-mercaptoethanol, and 0.01% bromophenol blue) and the protein solutions were then denatured on heating to boil for 3 min. The samples were then analyzed by SDS−PAGE. Protein samples were subjected to a discontinuous SDS−PAGE (2% acrylamide for the stacking gel and 10% acrylamide for the separation gel)[66] in a Genei vertical gel electrophoresis apparatus, carrying out the experiments at 50 V (stacking) and 100 V (separation). The gels were stained with Coomassie Brilliant Blue R-250 solution and destained with a water/methanol/acetic acid mixture for 3 h. The gels, after destaining, were scanned with a HP Precision Scan LTX scanner, and the images were further processed using Adobe Photoshop 7.0 software. Molecular weight markers were used to calibrate the molecular weights of the BSA. In order to identify the ROS involved in the cleavage reaction the radical scavengers such as hydroxyl radical (DMSO, 6 μL), singlet oxygen (NaN_3, 100 μM), superoxide (SOD, 4 unit), and H_2O_2 (catalase, 6 unit) were introduced.

Cell Culture. The SiHa human cervical cancer cell line was obtained from the National Center for Cell Science (NCCS), Pune, India. The cells were cultured in RPMI 1640 medium (Biochrom AG, Berlin, Germany) supplemented with 10% fetal bovine serum (Sigma), cisplatin (Getwell pharmaceuticals, India), and 100 U/mL penicillin and 100 μg/mL streptomycin as antibiotics (Himedia, Mumbai, India) in 96-well culture plates at 37 °C under a humidified atmosphere of 2% CO_2 in a CO_2 incubator (Heraeus, Hanau, Germany). All experiments were performed using cells from passage 15 or less.

Cell Viability Assay. MTT assay was carried out as described previously.[67] The complexes **1**−**4**, in the concentration range 0.05−50 μM, dissolved in 2% DMF: 5 mM Tris-HCl/50 mM NaCl buffer at pH 7.1 were added to the wells 24 h after seeding of 5×10^3 cells per well in 200 μL of fresh culture medium. After 24 and 48 h, 20 μL of MTT solution [5 mg/mL in phosphate-buffered saline (PBS)] was added to each well and the plates were wrapped with aluminum foil and incubated for 4 h at 37 °C. The purple formazan product was dissolved by addition of 100 μL of DMSO to each well. The absorbance was monitored at 570 nm (measurement) and 630 nm (reference) using a 96-well plate reader (Bio-Rad, Hercules, CA, USA). Data were collected for three replicates each and used to calculate the mean. The percentage inhibition was calculated, from this data, using the formula:

$$= \frac{\text{mean OD of untreated cells (control)} - \text{mean OD of treated cells}}{\text{mean OD of untreated cells (control)}} \times 100$$

The IC_{50} values were calculated using Table *Curve 2D*, version 5.01.

Hoechst 33258 Staining. Cell pathology was detected by staining the nuclear chromatin of trypsinized cells (4.0×10^4/mL) with 1 μL of Hoechst 33258 (1 mg/mL) for 10 min at 37 °C. Staining of suspension cells with Hoechst 33258 detected apoptosis.[68] A drop of cell suspension was placed on a glass slide and a coverslip was laid over to reduce light diffraction. At random 300 cells were observed in a fluorescent microscope (Carl Zeiss, Jena, Germany) fitted with a 377−355 nm filter and observed at ×400 magnification, and the percentage of cells reflecting pathological changes were calculated. Data were collected for triplicates and used to calculate the mean and the standard deviation.

AO/EB Staining. For both suspension and adherent cells, 96-well plates were centrifuged at 1000 rpm (129 g) for 5 min using a Beckman model TJ-6 centrifuge with inserts for 96-well plates. Acridine orange/ethidium bromide (AO/EB) dye mix (8 μL) was added to each well, and cells were viewed under the same microscope as above. Tests were done in triplicate, counting a minimum of 100 total cells each.

Comet Assay. DNA damage was quantified by adopting comet assay as previously described.[69,70] Assays were performed under red light at 4 °C. Cells used for the comet assay were sampled from a monolayer during the growth phase 24 h after seeding. Cells were treated with the complexes at IC_{50} concentration, and cells were harvested by a trypsinization process at 12 and 24 h. Normal agarose in PBS (200 μL of 1% solution) at 65 °C was dropped gently onto a fully frosted micro slide, covered immediately with a coverslip, and then placed over a frozen ice pack for ∼5 min. The coverslip was removed after the gel had set. The cell suspension from each cell fraction, in duplicate, was mixed with 1% low melting agarose at 37 °C in a 1:3 ratio. This mixture (100 μL) was quickly applied on top of the gel, coated over the micro slide, and allowed to set as before. A third coating of 100 μL 1% low melting agarose was given on the gel containing the cell suspension and allowed to set. After solidification of the agarose, the coverslips were removed, and the slides were immersed in ice-cold lysis solution (2.5 M NaCl, 100 mM Na_2EDTA, 10 mM Tris, NaOH: pH 10, 0.1% Triton X-100) and placed in a refrigerator at 4 °C for 16 h. All of the above operations were performed under low lighting conditions to avoid DNA damage due to light. The slides, after being removed from the lysis solution, were placed horizontally in an electrophoresis tank. The reservoirs were filled with electrophoresis buffer (300 mM NaOH, 1 mM Na_2EDTA, pH > 13) until the slides were just immersed in it. The slides were allowed to stand in the buffer for 20 min (to allow DNA unwinding), after which electrophoresis was carried out at 0.8 V/cm for 15 min. After electrophoresis, the slides were removed, washed thrice in neutralization buffer (0.4 M Tris, pH 7.5), and gently tapped to dry. Nuclear DNA was stained with 20 μL of ethidium bromide (50 μg/mL). Photographs were obtained using an epifluorescence microscope (Carl Zeiss). From each treatment, 200 cells were digitalized and analyzed with image analysis software (CASP software). The images were used to determine the DNA content of individual nuclei and to evaluate the degree of DNA damage representing the fraction of total DNA in the tail.

Determination of Intracellular Reactive Oxygen Species (ROS). The production of intracellular ROS was measured using the fluorescent probe 2′,7′-dichlorofluorescein diacetate (DCFH-DA). DCFH-DA diffuses through the cell membrane and is enzymatically hydrolyzed by intracellular esterases to form the non-nonfluorescent compound 2′,7′-dichlorofluorescein (DCFH), which is then rapidly oxidized to form the highly fluorescent 2′,7′-dichlorofluorescin (DCF) in the presence of ROS.[71] The DCF fluorescence intensity is believed to parallel the amount of ROS formed intracellularly. The cultured cancerous cells were treated with IC_{50} concentration of copper complexes **1**−**4** and the untreated cells were maintained as control. After 12 h the cells were incubated with 10 μM of DCFH-DA at 37 °C. After the incubation with DCFH-DA, the fluorescence intensity was measured at 485 nm excitation and 530 nm emission. As a positive control, the SiHa cancer cells have been exposed to 100 μM H_2O_2 for 30 min. Significant DCF staining is observed for this control.

RESULTS AND DISCUSSION

Structures of Copper(II) Complexes in Solution. The mixed ligand complexes $[Cu(bba)(diimine)](ClO_4)_2$ **1**−**4**, where bba is *N*,*N*′-bis(benzimidazol-2-ylmethyl)amine and diimine is 2,2′-bipyridine (bpy, **1**), 1,10-phenanthroline (phen, **2**), 5,6-dimethyl-1,10-phenanthroline (5,6-dmp, **3**), or dipyrido[3,2-*d*:2′,3′-*f*]quinoxaline (dpq, **4**), have been isolated. The formula of the complexes $[Cu(bba)(diimine)](ClO_4)_2$ **1**−**4**, as determined by elemental analysis, is supported by the X-ray crystal structures of **2** and **3** (cf. below). The absorption spectra of all the complexes in the solid state exhibit only one broad ligand field band in the visible region (550−620 nm), which is characteristic of Cu(II) located in a square-based environment.[50] On dissolution in acetonitrile the band is shifted to longer wavelength (612−617 nm) for **1**−**3** with very low absorptivity; in contrast, a blue-shift (6 nm) is observed for **4**.

dx.doi.org/10.1021/ic2017177 | *Inorg. Chem.* 2012, 51, 5512−5532

These observations suggest the presence of the same Cu(II) coordination geometry with small to large changes in the coordination sphere due to solvent coordination for all the complexes. On dissolution in 2% DMF - 5 mM Tris-HCl/50 mM NaCl buffer solution (pH, 7.2), all the complexes exhibit only one broad ligand field band at longer wavelengths (635−680 nm) and the red-shifts observed (23−66 nm) reveal significant changes in the coordination geometry, due to axial interaction of chloride ions available in high concentration. The intense absorption band observed in the UV region (224−294 nm) is attributed to the intraligand $\pi \rightarrow \pi^*$ transition located on the coordinated bba and diimine ligands (Table 1).

Table 1. Electronic Absorption Spectral Data of Cu(II) Complexes

		λ_{max}, nm (ε, M^{-1} cm^{-1})		
complexes	medium	ligand field[d]	ligand based[e]	
$[Cu(bba)(bpy))]^{2+}$ (**1**)	buffer[a]	635 (58)	277 (11300)	224 (7430)
	ACN[b]	602 (70)	271 (19520)	
	solid[c]	550		
$[Cu(bba)(phen)]^{2+}$ (**2**)	buffer[a]	638 (66)	270 (35500)	230 (10930)
	ACN[b]	613 (58)	270 (46710)	
	solid[c]	550		
$[Cu(bba)(5,6\text{-}dmp)]^{2+}$ (**3**)	buffer[a]	639 (48)	278 (35400)	230 (9930)
	ACN[b]	617 (62)	279 (38620)	
	solid[c]	605		
$[Cu(bba)(dpq)]^{2+}$ (**4**)	buffer[a]	680 (52)	294 (26900)	258 (52360)
	ACN[b]	614 (73)	256 (54240)	
	solid[c]	550		

[a]In 10% DMF/5 mM Tris-HCl/50 mM NaCl buffer (pH 7.1). [b]In acetonitrile. [c]Solid state (Nujol mull). [d]Concentration, 5×10^{-3} M. [e]Concentration, 2×10^{-5} M.

The polycrystalline and frozen solution EPR spectra (Figure S1, Table 2) of the complexes are axial with $g_{\parallel} > g_{\perp} > 2.0$ and $G = [(g_{\parallel} - 2)/(g_{\perp} - 2)] = 3.7-4.6$. The values of $g_{\parallel}$ and $A_{\parallel}$ obtained for frozen solutions are almost the same as those obtained for polycrystalline samples, revealing that the complexes do not undergo any major structural change upon dissolution. A square-based CuN_4 chromophore is expected[72,73] to show a $g_{\parallel}$ value of 2.200 and $A_{\parallel}$ value in the range 180−200 $\times 10^{-4}$ cm^{-1}, and a tetrahedral distortion from square planar coordination geometry or axial interaction would increase both the ligand field band position (cf. above) and $g_{\parallel}$ value and decrease the $A_{\parallel}$ value.[72,73] So, the observed values of $g_{\parallel}$ (2.221−2.230) and $A_{\parallel}$ (~182 $\times 10^{-4}$ cm^{-1}) for **1**−**4** are consistent with the presence of a square-based CuN_4 chromophore with no significant distortion from planarity, as evident from the crystal structure of **2** (cf below). This is supported by the values of $g_{\parallel}/A_{\parallel}$ quotient, which fall within the range expected for square planar geometry (120−132 cm). The ESI−MS data reveal that the complexes retain their identity even in solution (Figure S2, Supporting Information), and this is supported by values of molar conductivity in acetonitrile (Λ_M/Ω^{-1} cm^2 mol^{-1}: 218−222), which falls in the range[72] for 1:2 electrolytes. The cyclic (CV) and differential pulse voltammetric (DPV) responses obtained in methanol solution reveal that the Cu(II)/Cu(I) redox couple of **1**−**4** are far from reversible (Table S1, $E_{1/2}$, −0.104 to −0.426 V; ΔE_p, 90−140 mV, Figure S3). The $E_{1/2}$ values follow the trend **4** > **3** ≥ **2** ≥ **1**, which is consistent with the ability of the more π-delocalized quinoxaline ring in **4** to stabilize Cu(I) oxidation state more than that of the phen ring in **2**, and that of the electron-releasing methyl groups on 5,6 positions in **3** to stabilize Cu(II) oxidation state more than the bpy ring in **1**.

Structures of $[Cu(bba)(phen)](ClO_4)_2 \cdot CH_3OH$ 2 and $[Cu(bba)(5,6\text{-}dmp)]\text{-}(ClO_4)_2 \cdot (H_2O) \cdot (CH_3OCH_3)$ 3. In the crystallographic asymmetric unit cell of **2** are present a discrete monomeric copper(II) complex dication, two perchlorate anions and one lattice MeOH molecule. The ORTEP view of the structure of the complex cation $[Cu(bba)(phen)]^{2+}$, along with the atom numbering scheme, is shown in Figure 1. The crystallographic data are given in Table 3, and the selected bond distances and bond angles relevant to the copper coordination sphere are given in Table 4. The value of the

Table 2. Electron Paramagnetic Resonance Spectral Data for the Cu(II) Complexes

complexes	medium[e]	$g_{\parallel}$	$g_{\perp}$	$A_{\parallel}$[a]	$g_{\parallel}/A_{\parallel}$	G	g_0[b]	A_0[b]	$g_{\perp}$[c]	$A_{\perp}$[c]
$[Cu(bba)(bpy))]^{2+}$ (**1**)	*Pc* (RT)	*d*	2.045							
	Pc (LNT)	*d*	2.068							
	frozen solution	2.221	2.056	182	122	3.95			2.056	23
	solution (RT)						2.114	76		
$[Cu(bba)(phen)]^{2+}$ (**2**)	*Pc* (RT)	*d*	2.045							
	Pc (LNT)	*d*	2.073							
	frozen solution	2.230	2.049	183	122	4.69			2.068	22.5
	solution (RT)						2.120	76		
$[Cu(bba)(5,6\text{-}dmp)]^{2+}$ (**3**)	*Pc* (RT)	2.227	2.045	185	120	3.66				
	Pc (LNT)	*d*	2.047							
	frozen solution	2.224	2.059	183	122	3.80			2.060	34.5
	solution (RT)						2.117	84		
$[Cu(bba)(dpq)]^{2+}$ (**4**)	*Pc* (RT)	2.232	2.044	177	126	4.07				
	Pc (LNT)	*d*	2.068							
	frozen solution	2.228	2.057	183	122	4.00			2.061	33
	solution (RT)						2.117	84		

[a]$A_{\parallel}$ and A_0 in 10^{-4} cm^{-1}; $g_{\parallel}/A_{\parallel}$ in cm. [b]g_0 and A_0 obtained from solution spectrum at room temperature; solution in 10% DMF/5 mM Tris-HCl/50 mM NaCl buffer. [c]$g_{\perp}$ and $A_{\perp}$ computed as $^1/_2(3g_0 - g_{\parallel})$ and $^1/_2(3A_0 - A_{\parallel})$, respectively. [d]Broadened. [e]*Pc*, polycrystalline. Frozen solution: In 10% DMF/5 mM Tris-HCl/50 mM NaCl buffer (pH 7.1)/acetone (4:1 v/v) glass at 77 K. $A_{\parallel}$ in 10^{-4} cm^{-1} at liquid nitrogen temperature (77 K).

dx.doi.org/10.1021/ic2017177 | *Inorg. Chem.* 2012, 51, 5512−5532

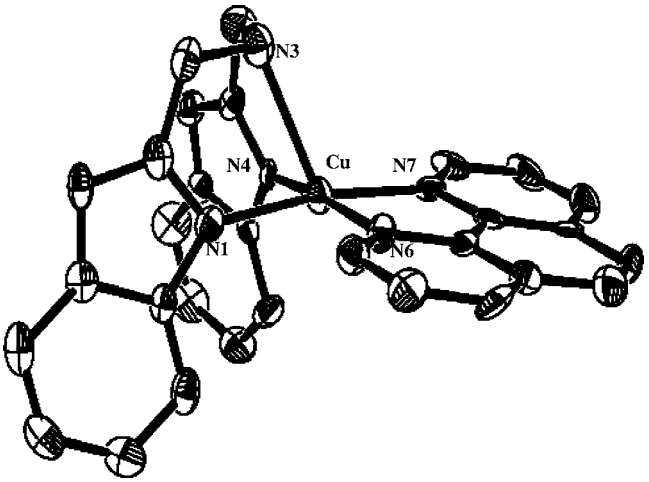

Figure 1. ORTEP representation of the crystal structure of $[Cu(bba)(phen)](ClO_4)_2 \cdot MeOH$ showing atom numbering scheme and displacement ellipsoid (50% probability level). (Hydrogen atoms, perchlorate anions, and lattice methanol are omitted for clarity).

Table 3. Crystal Data and Structure Refinement Details for Complexes 2 and 3

	2	3
empirical formula	$C_{29}H_{27}Cl_2CuN_7O_9$	$C_{34}H_{39}Cl_2CuN_7O_{10}$
formula weight	752.02	840.16
crystal system	monoclinic	monoclinic
space group	*P*21/*n*	*P*21/*n*
a, Å	18.5438(17)	13.3357(4)
b, Å	9.5229(9)	17.1139(5)
c, Å	19.5434(17)	17.4396(5)
α, deg	90	90.00
β, deg	117.3410(10)	107.5180(10
γ, deg	90	90.00
V, Å	3065.6(5)	3795.58(19)
Z	4	4
λ, Å (Mo K*α*)	0.71073	0.71073
D_{calc}, g·cm^{-3}	1.629	1.470
goodness-of-fit on F^2	1.265	1.033
θ for data collection (deg)	2.06−25.00	1.70−26.28
final *R* indices [$I > 2\sigma(I)$]	R_1 = 0.1038, wR_2 = 0.1993	R_1 = 0.0554, wR_2 =0.1488
R_1[a]	0.1239	0.0862
wR_2[a]	0.2087	0.1711

[a] $R_1 = \Sigma \, ||F_o| - |F_c||/\Sigma|F_o|$, $wR_2 = \{\Sigma w[(F_o^2 - F_c^2)^2/\Sigma w[(F_o^2)^2]\}^{1/2}$.

structural index[74] τ of 0.03 [$\tau = (\beta - \alpha)/60$, where α = N4−Cu1−N6 = 172.3° and β = N1−Cu1−N7 = 170.4°; for perfect square pyramidal and trigonal bipyramidal geometries the τ values are zero and unity, respectively] reveals that the coordination geometry around copper(II) is best described as square pyramidal[75−77] with no significant distortion toward trigonal bipyramidal. The tridentate ligand bba is bound facially to Cu(II) with the two bzim nitrogens (Cu−N_{bzim}, 1.979(6), 1.999(6) Å) located in the basal plane and the two imine nitrogens of phen (Cu−N_{imine}, 2.001(6), 2.034(6) Å) occupying the remaining corners of the basal plane. The strongly bound phen nitrogens occupy the equatorial sites around Cu(II) with the sterically hindered N3 amine nitrogen atom of bba defaulting to the more weakly bound *z*-axial position (Cu(1)−N(3), 2.477(6) Å).[78] The displacement of copper atom above the N1N4N7N6 plane is 0.136 Å illustrating the importance of the steric effect of the bulky bzim moieties. The Cu−N_{bzim} and Cu−N_{imine} bond distances are similar to those observed for $[Cu(bba)Cl_2]$[46] and $[Cu(bba)_2]^{2+}$.[78] The Cu−$N7_{phen}$ bond (2.001(6) Å) is shorter than the Cu−$N6_{phen}$ bond (2.034(6) Å), as it is trans to the longer Cu−N_{amine} bond. The axial Cu−N_{amine} bond is longer than the equatorial Cu−N_{phen} bonds, which is expected of the presence of two electrons in the d_z^2 orbital of Cu(II).

Table 4. Selected Interatomic Distances [Å] and Bond Angles [deg] for Complexes 2 and 3

2		3	
Bond Lengths [Å]			
Cu(1)−N(1)	1.979(6)	Cu(1)−N(1)	1.981(3)
Cu(1)−N(4)	1.999(6)	Cu(1)−N(4)	1.982(3)
Cu(1)−N(7)	2.001(6)	Cu(1)−N(7)	2.011(3)
Cu(1)−N(6)	2.034(6)	Cu(1)−N(3)	2.066(3)
Cu(1)−N(3)	2.477(6)	Cu(1)−N(6)	2.206(3)
Bond Angles [deg]			
N(1)−Cu(1)−N(4)	89.1(2)	N(1)−Cu(1)−N(4)	151.77(12)
N(1)−Cu(1)−N(7)	170.4(2)	N(1)−Cu(1)−N(7)	98.64(12)
N(4)−Cu(1)−N(7)	94.5(2)	N(4)−Cu(1)−N(7)	98.64(12)
N(1)−Cu(1)−N(6)	93.8(2)	N(1)−Cu(1)−N(3)	83.03(13)
N(4)−Cu(1)−N(6)	172.3(2)	N(4)−Cu(1)−N(3)	80.83(13)
N(7)−Cu(1)−N(6)	81.6(2)	N(7)−Cu(1)−N(3)	178.29(13)
N(1)−Cu(1)−N(3)	77.5(2)	N(1)−Cu(1)−N(6)	99.44(12)
N(4)−Cu(1)−N(3)	77.5(2)	N(4)−Cu(1)−N(6)	106.36(12)
N(7)−Cu(1)−N(3)	112.0(2)	N(7)−Cu(1)−N(6)	78.66(11)
N(6)−Cu(1)−N(3)	110.2(2)	N(3)−Cu(1)−N(6)	101.45(13)

The X-ray crystal structure of **3** consists of a discrete monomeric complex dication $[Cu(bba)(5,6\text{-dmp})]^{2+}$, two perchlorate anions, one lattice water and a dimethyl ether molecule in the crystallographic asymmetric unit cell. The ORTEP view of the dication, along with the atom numbering scheme, is shown in Figure 2, and the selected bond distances and bond angles relevant to the copper coordination sphere are given in Table 4. The tridentate bba and bidentate 5,6-dmp ligands are bound to Cu(II) in the complex cation. The value of the structural index[74] τ of 0.44 suggests that the coordination geometry around copper(II) is best described as trigonal bipyramidal distorted square based pyramidal (TBDSBP)[75−77] and that the steric congestion at Cu(II) in **3** is higher than that in **2**. This is supported by the displacement of the copper atom above the mean plane N1N3N4N7 (0.195 Å), which is higher than that in **2**. Also, in contrast to **2**, the bba ligand in **3** is bound meridionally to Cu(II) with the two bzim nitrogens (Cu−N_{bzim}, 1.981(3), 1.982(3) Å) and the N3 amine nitrogen atom (Cu(1)−N(3), 2.066(3) Å) occupying the three corners of the basal plane. The N7 imine nitrogen of 5,6-dmp (Cu−$N7_{imine}$, 2.012 Å) is located at the remaining corner of the basal plane. The other imine nitrogen (N6) is located in the apical position at a distance (Cu(1)−N(6), 2.207(3) Å) longer than the equatorial one due to the presence of two electrons in the d_z^2 orbital of Cu(II). This is in contrast to the occupation of both the imine nitrogens in the basal plane of **2**. It appears that the strong equatorial coordination of one of the nitrogens of 5,6-dmp to Cu(II) weakens the donor ability of the other nitrogen leading to stabilize the equatorial, axial coordination of the co-ligand in **3** unlike the parent ligand phen in **2** and hence the meridional coordination of bba in **3** in the solid state. Also, the imine nitrogen N(6) in **3** is located at a distance shorter

dx.doi.org/10.1021/ic2017177 | *Inorg. Chem.* 2012, 51, 5512−5532

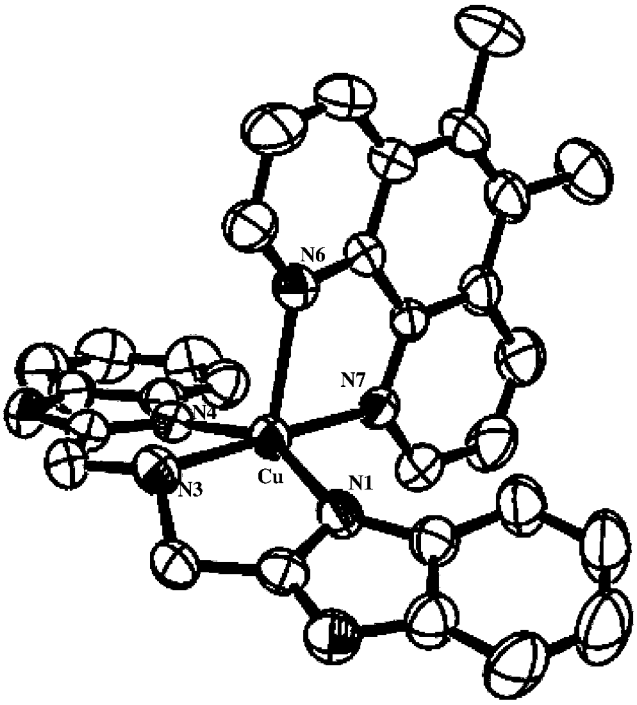

Figure 2. ORTEP representation of the crystal structure of $[Cu(bba)(5,6\text{-dmp})](ClO_4)_2 \cdot H_2O \cdot C_2H_5OC_2H_5$ showing atom numbering scheme and displacement ellipsoid (50% probability level) (hydrogen atoms, perchlorate anions, lattice water, and diethyl ether are omitted for clarity).

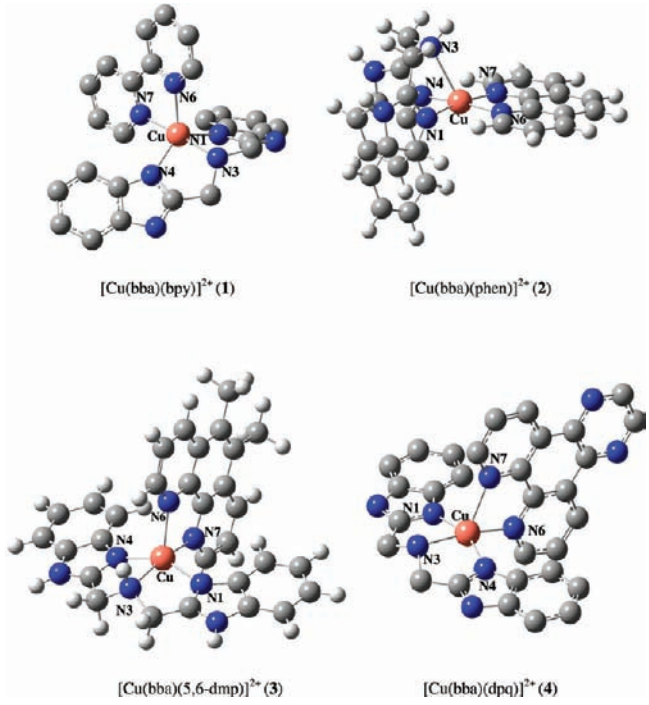

Figure 3. LANL2DZ and 6-31G(d,p) ground state optimized geometry of $[Cu(bba)(bpy)]^{2+}$ (**1**), $[Cu(bba)(phen)]^{2+}$ (**2**), $[Cu(bba)(5,6\text{-dmp})]^{2+}$ (**3**), and $[Cu(bba)(dpq)]^{2+}$ (**4**).

than that in **2**, which is consistent with the higher τ value as well as displacement of copper from the 4N coordination plane.

Structures of Complexes: Density Functional Theory Calculations. Geometry optimization and frequency calculations for **1**−**4** have been carried out at DFT level. The Cu atom was described using the LANL2DZ basis set while all the nonmetal atoms were described using the 6-31G* basis set (Figure 3). The initial geometries were taken from the single-crystal X-ray data of $[Cu(bba)(phen)]^{2+}$ **2** and subjected to optimization. The geometrical parameters viz. bond lengths, bond angles and bond energies were calculated (Table S2, Supporting Information) using Gaussian 03 package. Contour plots of molecular orbitals of the complexes were generated using Gauss view 3.0 and the frontier molecular orbitals in **1**−**4** were calculated (Figure 5). As the DFT calculations reproduce the experimental structures of **2** and **3**, the optimized structures of **1** and **4** are valid. Interestingly, the ligand bba is coordinated facially to Cu(II) in the X-ray structure of **2** but meridionally in the X-ray structure of **3** as well as in the optimized structures of **1** and **4**. The value of the structural index[74] τ in the optimized structure of **3** is 0.29, which is lower than that (τ, 0.44) experimentally observed. The value of τ for **4** (0.23) and **1** (0.80) suggest that the geometries of the complexes are respectively trigonal bipyramidal distorted square based pyramidal (TBDSBP) and square based pyramidal distorted trigonal bipyramidal (SBPDTB).

It is seen that the singly occupied molecular orbital (SOMO) is localized largely on the bzim moieties in **1**−**4**, and the calculated energy of SOMO varies as **4** (−11.5386) > **3** (−11.8814) > **1** (−11.9813) > **2** (−12.1002 eV). Frontier molecular orbital approximation indicates that SOMO accounts for the electron-donating ability of the ligand, the highest value of SOMO energy of **4** revealing that the bzim ligand moieties in the complex release electrons into the unoccupied orbital of the metal ion, and hence are involved in the strongest σ-bonding to Cu(II). Thus the donor ability of the primary ligand bba is modified by the variation in the diimine co-ligand, which reflects the presence of synergy between the primary and secondary ligands. The energy of SOMO+1 localized largely on the diimine co-ligand corresponds to the ability of the co-ligand to accept electrons, and the observed trend in energy of the SOMO+1, **1** (−7.29899) > **2** (−8.08051 eV) < **3** (−7.42961) > **4** (−7.66989) illustrates the stronger involvement of the more delocalized π^* orbital of dpq co-ligand in **4** in π back-bonding with copper to stabilize Cu(I) oxidation state more than bpy and 5,6-dmp co-ligands and encourage stronger coordination of bba. This is in good agreement with the observed order of $E_{1/2}$ values of the complexes, except the phen complex **2**, the more π-delocalized dpq ring in **4** stabilizing the Cu(I) oxidation state more than the bpy ring in **1**. The order of energy of SOMO+1 suggests that the phen co-ligand in **2** is expected to be involved in stronger π back-bonding with copper to stabilize the Cu(I) oxidation state more than the dpq co-ligand, leading to a $E_{1/2}$ value for **2** higher than **4**. However, the observed $E_{1/2}$ value of **2** is lower than that of **4**, illustrating that the phen complex **2** assumes a coordination geometry with meridional coordination of bba in solution, like all the other complexes. This is supported by the similar solution spectral data of the complexes. The lowest SOMO energy calculated for **2** with facial coordination of bba means that the strong equatorial coordination of phen stabilizes the facial coordination of bba in the solid state, which rearranges to meridional coordination upon dissolution in acetonitrile. Interestingly, DFT calculations show that gas phase geometry of **2** (τ, 0.01) changes to one (τ, 0.19) with meridional coordination of bba (Figure 4, Table S2). Also, the highest DNA binding affinity of **4** is due to the strongest π-stacking interaction of the dpq ring in between the

dx.doi.org/10.1021/ic2017177 | Inorg. Chem. 2012, 51, 5512−5532

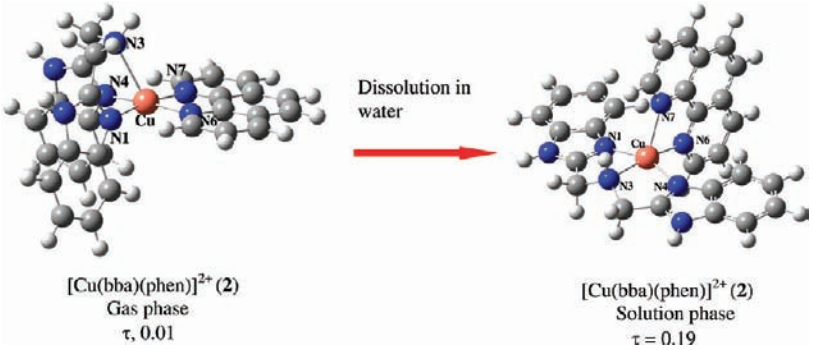

Figure 4. LANL2DZ and 6-31G(d,p) ground state optimized geometry of $[Cu(bba)(phen)]^{2+}$ (**2**) both in the gas phase and solution phase (water as medium).

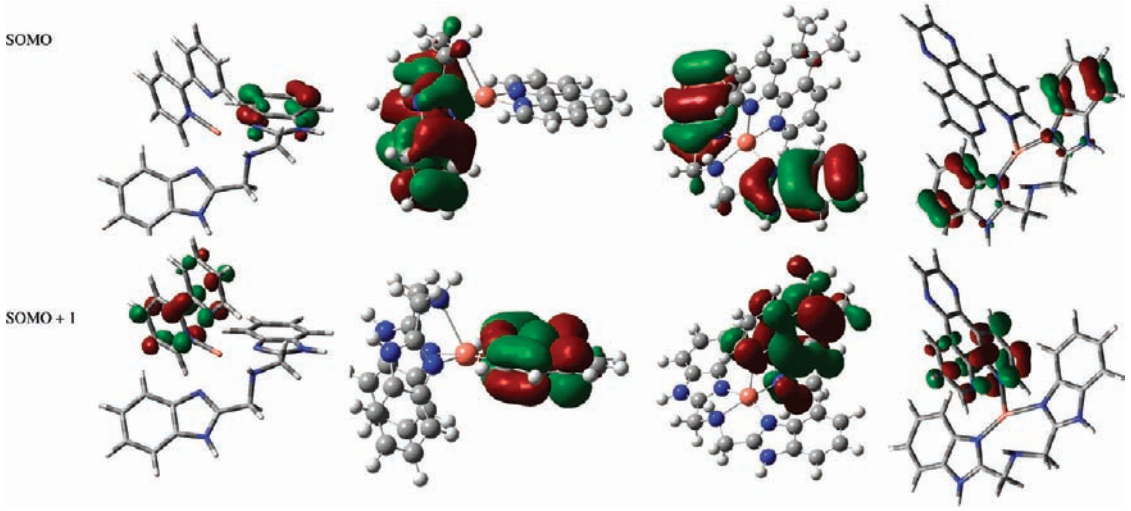

Figure 5. Frontier orbitals diagram for the SOMO and SOMO+1 of **1**−**4**.

DNA base pairs with the SOMO+1 of dpq interacting more strongly with the filled orbital of nucleobases than other diimines (cf below).

DNA Binding Studies. Upon the incremental addition of CT DNA to the complexes **1**−**4** the ligand centered $\pi \rightarrow \pi^*$ absorption band (258−278 nm) shows increasing hypochromism ($\Delta\varepsilon$, 72−82%) with no red-shift (Figure S4, Supporting Information). As the extent of hypochromism is commonly associated with the strength of DNA interaction,[32] the observed decrease in order of hypochromism, **4** > **3** > **2** > **1**, reflects the decrease in DNA binding affinities of the complexes in this order. The DNA binding affinities of **1**−**4** are compared quantitatively by obtaining the intrinsic binding constant K_b using the equation

$$[DNA]/(\varepsilon_a - \varepsilon_f) = [DNA]/(\varepsilon_b - \varepsilon_f) + 1/K_b(\varepsilon_a - \varepsilon_f)$$

where [DNA] is the concentration of DNA in base-pairs, ε_a is the apparent extinction coefficient obtained by calculating A_{obs}/[complex], ε_f is the extinction coefficient of the complex in its free form, and ε_b is the extinction coefficient of the complex in the bound form. Each set of data, when fitted into the above equation, gave a straight line with a slope of $1/(\varepsilon_b - \varepsilon_f)$ and an y-intercept of $1/K_b(\varepsilon_b - \varepsilon_f)$ and the value of K_b was determined from the ratio of slope to intercept (Figure 6A,B). The observed K_b values ($0.06-2.20 \times 10^5$ M^{-1}, Table 5) are higher than those of $[Cu(bba)Cl_2]$[79] and $[Cu(L)(phen)]^+$, where L is 1,2-bis(1H-benzimidazol-2-yl)ethane-1,2-diol,[79] and $[VO(bba)(diimine)]Cl_2$[78] and vary as **4** > **3** > **2** > **1**. The highest DNA binding affinity of **4** is attributed to the dpq co-ligand, the extended aromatic ring surface of which facilitates its π-stacking interaction with DNA base pairs. The complex **2** shows DNA binding affinity lower than **4** revealing that the phen ring is involved in weaker π-stacking interaction with DNA base pairs. As bpy ligand lacks a larger planar aromatic ring surface, **1** is involved in a weaker electrostatic interaction through the negatively charged phosphate groups on the DNA surface. The two methyl groups on 5,6 positions of the phen ring in **3** would sterically discourage π-stacking of the ring with DNA base pairs, and so they are involved in hydrophobic interaction with the DNA surface rather than partial intercalative interaction leading to a DNA binding affinity higher than that for its phen analogue. Similar observations have been made by us earlier for the mononuclear tris-complexes $[Cu(5,6\text{-dmp})_3]^{2+}$, $[Zn(5,6\text{-dmp})_3]^{2+}$,[80] and $[Ru(5,6\text{-dmp})_3]^{2+}$,[81] the mixed ligand complexes $[Ru(NH_3)_4(5,6\text{-dmp})]^{2+}$,[84] $[Cu(imda)(5,6\text{-dmp})]$,[41] $[Cu(dipica)(5,6\text{-dmp})]^{2+}$,[82] and $[Cu(L\text{-tyr})(5,6\text{-dmp})]^+$,[32] and the dinuclear complexes $[\{(5,6\text{-dmp})_2Ru\}_2(bpm)]^{4+}$[83] and $[Cu_2(LH)_2(5,6\text{-dmp})(ClO_4)_2]^{2+}$[47] bound to CT DNA, all of them containing 5,6-dmp as the co-ligand. Upon replacing the pyridyl moieties in $[Cu(dipica)(diimine)]^{2+}$[82] by bzim moieties as in $[Cu(bba)(diimine)]^{2+}$, **1**−**4** the DNA binding affinity increases by 10−100 fold. The hydrophobic[12] interaction of bzim moieties with the DNA surface is expected to contribute significantly to the higher DNA binding affinities of the bba complexes, and

dx.doi.org/10.1021/ic2017177 | Inorg. Chem. 2012, 51, 5512−5532

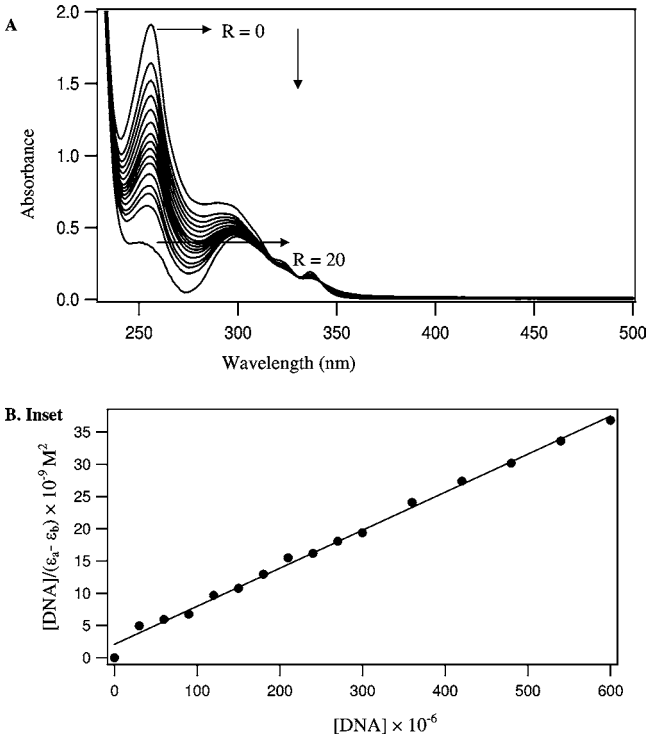

Figure 6. (A) Absorption spectra of $[Cu(bba)(dpq)]^{2+}$ (2×10^{-5} M) in 2% DMF/5 mM Tris-HCl/50 mM NaCl buffer at pH 7.1 in the absence ($R = 0$) and presence ($R = 1 - 20$) of increasing amounts of CT DNA. (B) The plot of [DNA] vs $[DNA]/(\varepsilon_a - \varepsilon_b)$ at $R = 0 - 25$ of the complex $[Cu(bba)(dpq)]^{2+}$.

molecular model studies show no possibility for hydrogen bonding of bzim-NH with the nucleobases present on the edge of the DNA.[48] Thus, the partial intercalation of phen and dpq co-ligands and the hydrophobic interaction involving both the diimine co-ligands, as in Ru(II) arene complexes,[12] and the bzim moieties of the primary ligand are the useful features for incorporation into Cu(II) complexes to optimize their DNA recognition.

The trend in DNA binding affinities determined from absorption spectral studies is consistent with the order of decrease in the induced emission intensity of DNA-bound EB,[85] namely, **4** > **3** > **2** > **1**, and interestingly, a plot of K_b vs K_{app} is linear (Figures 7 and S5, Table 6, Supporting Information). Also, the ability of complexes to increase the viscosity of DNA (Figure 9, Supporting Information) depends upon the diimine co-ligand: dpq (**4**) ≥ 5,6-dmp (**3**) > phen (**2**) > bpy (**1**), which supports the DNA binding modes proposed (cf. above).

Circular Dichroic Spectral Studies. The CD spectrum of B DNA shows a positive band at 275 nm (UV: λ_{max}, 258 nm) arising due to base stacking and a negative band at 245 nm due

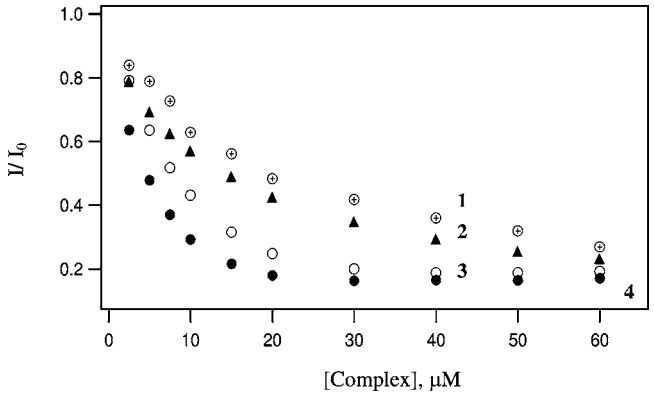

Figure 7. Effect of the addition of the complexes **1**−**4** on the emission intensity of the CT DNA-bound ethidium bromide at different complex concentrations in a 2% DMF/5 mM Tris-HCl/50 mM NaCl buffer at pH 7.1 and at 25 °C; the concentration of DNA is 125 μM, [EB] = 12.5 μM.

to helicity, which are very sensitive to the mode of DNA interaction of small molecules.[86] Thus, simple groove binding and electrostatic interaction of a small molecule with DNA exhibits a small or no perturbation on the base stacking and helicity bands of DNA, while intercalation enhances the intensities of both the bands stabilizing the right-handed B form of DNA as observed for the classical intercalator methylene blue.[87] When **1**−**4** are incubated with DNA at $1/R$ = [Cu complex]/[DNA]) = 1, the CD spectrum of DNA undergoes interesting changes in both the positive and negative bands (Figure 8, Table 6). The complexes **1**, **2**, and **4** show a slight decrease and increase in band intensities of respectively the negative and positive bands, indicating that the interaction of complexes disturbs the DNA helicity. Interestingly, the high-intensity bands for **2**, **3**, and **4** superposed on the broad positive band at 277, 288, and 274 nm, respectively, correspond to the positions of their UV absorption bands, and so they are induced CD (ICD) bands. Also, **3** shows a higher red-shift of nearly 13 nm for both the bands with large increase and large decrease in intensities respectively of the positive (ICD) and negative bands (Figure 8), which originate from the coupling of 5,6-dmp chromophore with those of DNA bases. This observation is consistent with a B to A conformational change[88] with the increased positive base pair tilting in A DNA caused by the hydrophobic interaction of 5,6-methyl groups with DNA. A similar red-shift (10 nm) observed for $[Cu(dipica)(5,6\text{-dmp})]^{2+}$ has been ascribed to a B to A conformational change.[82] Similar observations have been made by us earlier for mononuclear simple[50,80,81] and mixed ligand[41,82−84] and dinuclear[32] complexes of 5,6-dmp ligand bound to CT DNA.

DNA Cleavage Studies. *DNA Cleavage without Added Reductant.* In order to explore the DNA cleavage abilities of

Table 5. Absorption Spectral Properties of Cu(II) Complexes Bound[a] to CT DNA

complexes	λ_{max} (nm)	change in absorbance	$\Delta\varepsilon$ (%)	red shift (nm)	K_b (M^{-1})
$[Cu(bba)(bpy)]^{2+}$ (**1**)	277	hypochromism	70	0	$0.06 \pm 0.07 \times 10^5$
$[Cu(bba)(phen)]^{2+}$ (**2**)	270	hypochromism	76	0	$0.28 \pm 0.04 \times 10^5$
$[Cu(bba)(5,6\text{-dmp})]^{2+}$ (**3**)	278	hypochromism	80	0	$1.09 \pm 0.39 \times 10^5$
$[Cu(bba)(dpq)]^{2+}$ (**4**)	258	hypochromism	82	0	$2.20 \pm 0.34 \times 10^5$

[a]Measurement were made at R = [DNA]/[complex] = 20, concentration of solution of copper(II) complexes in buffer = 3×10^{-5} M (**1** and **2**) and 2.0×10^{-5} M (**3** and **4**).

dx.doi.org/10.1021/ic2017177 | Inorg. Chem. 2012, 51, 5512−5532

Table 6. Emission Spectral Properties and CD Parameters for the Interaction of Calf Thymus DNA and BSA with Copper(II) Complexes

complexes	K_{app} [a]	K_{sv} [b]	CD spectral band[c] wavelength (nm)			
			negative band	positive band	cross over point	UV band
CT DNA			245	275	258	260
$[Cu(bba)(bpy)))]^{2+}$ (**1**)	1.25×10^5	1.7×10^5	246	277	257	277
$[Cu(bba)(phen)]^{2+}$ (**2**)	1.66×10^5	3.6×10^5	247	278	256	270
$[Cu(bba)(5,6\text{-dmp})]^{2+}$ (**3**)	2.08×10^5	10.8×10^5	252	288	261	278
$[Cu(bba)(dpq)]^{2+}$ (**4**)	3.57×10^5	5.1×10^5	244	274	254	258

[a]Apparent DNA binding constant from ethidium bromide displacement assay. [b]BSA binding constant from tryptophan fluorescence quenching measurement. [c]Measurement made at $1/R$ = [Cu]/[NP] value of 1 for complexes **1**–**4**; concentration of DNA solutions = 2.5×10^{-5} M. Cell path length, 1 cm.

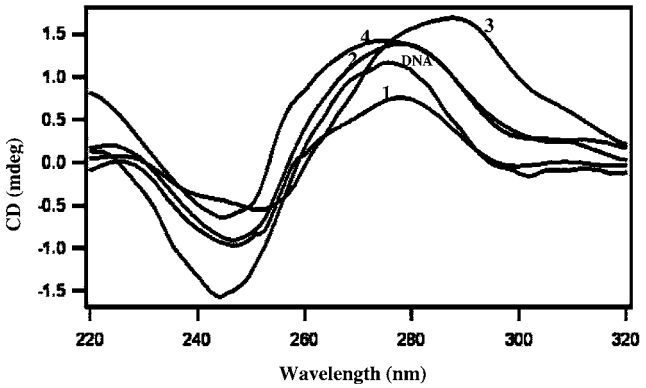

Figure 8. Circular dichroism spectra of CT DNA (4×10^{-4}) in 2% DMF/5 mM Tris-HCl/50 mM NaCl buffer at pH 7.1 and 25 °C in the absence (DNA) and presence of $[Cu(bba)(bpy)]^{2+}$ (**1**), $[Cu(bba)(phen)]^{2+}$ (**2**), $[Cu(bba)(5,6\text{-dmp})]^{2+}$ (**3**), and $[Cu(bba)(dpq)]^{2+}$ (**4**) at a $1/R$ value of 1.

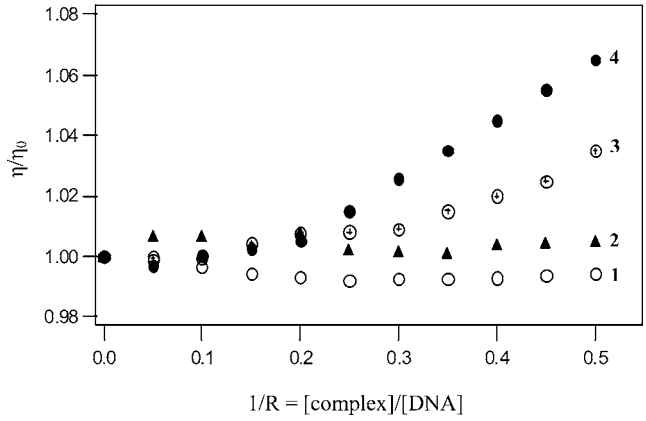

Figure 9. Effect of the complexes **1**–**4** on the viscosity of CT DNA. Relative specific viscosity versus $1/R$; [CT DNA] = 500 μM.

the complexes supercoiled (SC) pUC19 DNA (40 μM) was incubated with **1**–**4** in the absence of an activator in 2% DMF/5 mM Tris-HCl/50 mM NaCl buffer at pH 7.1 for 1 h at 37 °C. Only **4** shows prominent DNA cleavage to give nicked circular (NC) form (83%), while **1**–**3** and $[Cu(bba)Cl_2]$ fail to show any cleavage (Figure 10, Table 7). Control experiments with ligand or $Cu(ClO_4)_2 \cdot 6H_2O$ or DNA alone do not reveal any cleavage. The selective and effective DNA cleavage of **4** may be traced to the strongest DNA binding affinity and the highest Cu(II)/Cu(I) redox potential of the complex. Under both the "pseudo-Michaelis-Menten" and "true Michaelis-Menten"

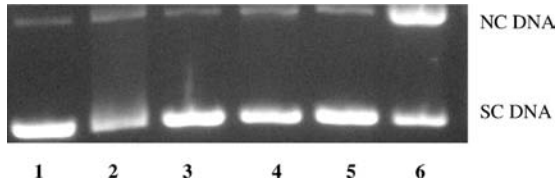

Figure 10. Cleavage of supercoiled pUC19 DNA (40 μM) by complexes **1**–**4** (100 μM) in a buffer containing 2% DMF:5 mM Tris HCl and 50 mM NaCl at pH = 7.1 and 37 °C with an incubation time of 1 h. Lane 1, DNA; lane 2, DNA + $[Cu(bba)Cl_2]$; lane 3, DNA + **1**; lane 4, DNA + **2**; lane 5, DNA + **3**; lane 6, DNA + **4**. Forms SC and NC are supercoiled and nicked circular DNA, respectively.

Table 7. Self-Activated Cleavage Data of SC pUC19 DNA (40 μM in base pair) by Complexes 1–4 (100 μM) in the Absence of Any Reducing Agent for Incubation Time of 1 h

serial no.	reaction conditions	form (%)	
		SC	NC
1	DNA control	94.6	5.4
2	DNA + $[Cu(bba)(Cl)_2]^{2+}$	77.0	23.0
3	DNA + **1**	93.1	6.9
4	DNA + **2**	87.9	12.1
5	DNA + **3**	89.3	10.7
6	DNA + **4**	17.0	83.0

conditions (Figures 11 and 12; Supporting Information), the rate of DNA cleavage in the presence of **4** is enormously enhanced over that of uncatalyzed DNA cleavage. Also, the extent of DNA cleavage varies exponentially with incubation time and follows pseudo-first-order kinetic profiles (Figure 13). The mechanism of DNA cleavage was studied by adding radical inhibitors to the reaction mixture (Figure S14A,B, Supporting Information). It was found that addition of DMSO significantly diminishes the nuclease activity indicating involvement of hydroxyl radicals in the cleavage process (Supporting Information). However, addition of distamycin, a DNA minor groove binder, does not inhibit the complex from cleaving DNA suggesting that the complex prefers to bind in the DNA major groove in the presence of distamycin.

DNA Cleavage with Ascorbic Acid Added as Reductant. The DNA strand scission by **1**–**4** (30 μM) was studied in the presence of ascorbic acid (Figure S6, Supporting Information). In control experiments with DNA or ascorbic acid alone, no DNA cleavage is observed. At lower complex concentrations, **4** (10 μM) and **2** (30 μM) convert SC DNA into NC form and then to linear open circular (LC) form revealing that both the complexes behave as chemical nucleases for

dx.doi.org/10.1021/ic2017177 | Inorg. Chem. 2012, 51, 5512–5532

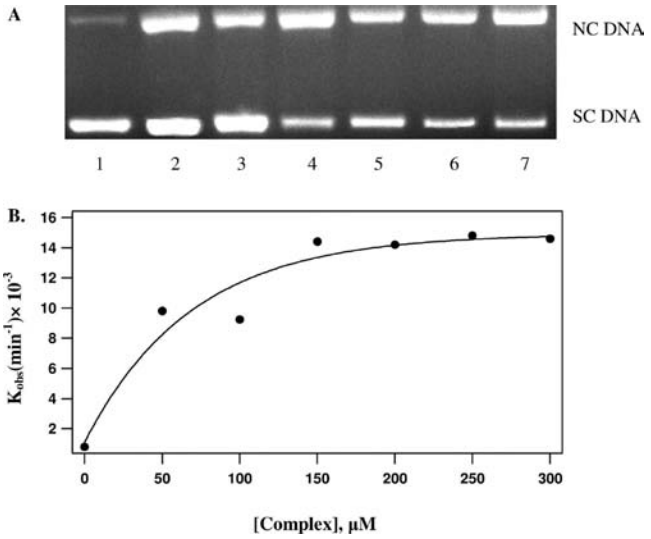

Figure 11. (A) DNA cleavage of supercoiled pUC19 DNA (40 μM) using various concentrations of complex **4** in a buffer containing 2% DMF:5 mM Tris HCl and 50 mM NaCl at pH = 7.1 and 37 °C with an incubation time of 1 h. Lane 1, DNA; lane 2, DNA + **4** (50 μM); lane 3, DNA + **4** (100 μM); lane 4, DNA + **4** (150 μM); lane 5, DNA + **4** (200 μM); lane 6, DNA + **4** (250 μM); lane 7, DNA + **4** (300 μM). Forms SC and NC are supercoiled and nicked circular DNA respectively. (B) Plot shows pseudo-Michaelis–Menten Kinetics of the cleavage of supercoiled pUC19 DNA with different complex concentrations of **4** (50–300 μM) for 1 h.

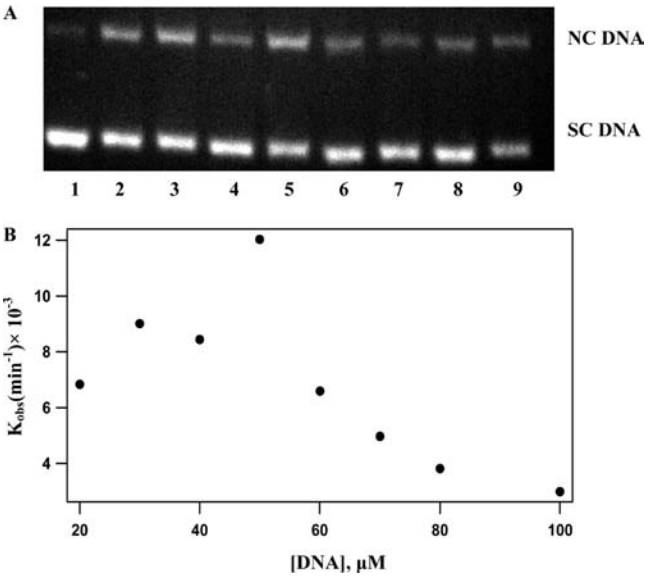

Figure 12. Saturation kinetics of DNA cleavage using various concentrations of supercoiled pUC19 DNA (40 μM) at constant concentration of complex **4** (80 μM) in a buffer containing 2% DMF:5 mM Tris HCl and 50 mM NaCl at pH = 7.1 and 37 °C with an incubation time of 1 h. Lane 1, DNA; lane 2, DNA (20 μM) + **4**; lane 3, DNA (30 μM) + **4**; lane 4, DNA (40 μM) + **4**; lane 5, DNA (50 μM) + **4**; lane 6, DNA (60 μM) + **4**; lane 7, DNA (70 μM) + **4**; lane 8, DNA (80 μM) + **4**; lane 9, DNA (100 μM) + **4**. Forms SC and NC are supercoiled and nicked circular DNA, respectively. (B) Plot shows saturation kinetics of the cleavage of supercoiled pUC19 DNA using 80 μM complex **4** with different concentrations of SC DNA (20–100 μM) for 1 h.

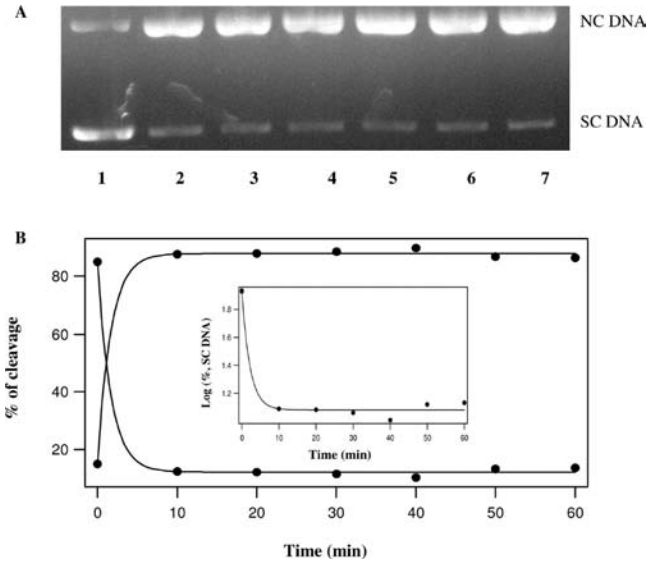

Figure 13. Time-dependent cleavage of supercoiled pUC19 DNA (40 μM) by the complex **4** (100 μM) in 2% DMF:5 mM Tris-HCl/50 mM NaCl at pH = 7.1 and at 37 °C Lane 1, DNA; lane 2, DNA + **4** (10 min); lane 3, DNA + **4** (20 min); lane 4, DNA + **4** (30 min); lane 5, DNA + **4** (40 min); lane 6, DNA + **4** (50 min); lane 7, DNA + **4** (60 min). Forms SC and NC are supercoiled and nicked circular DNA, respectively. (B) Plot shows log (% SC DNA) vs time for complex **4** (100 μM) for an incubation period of 0–60 min.

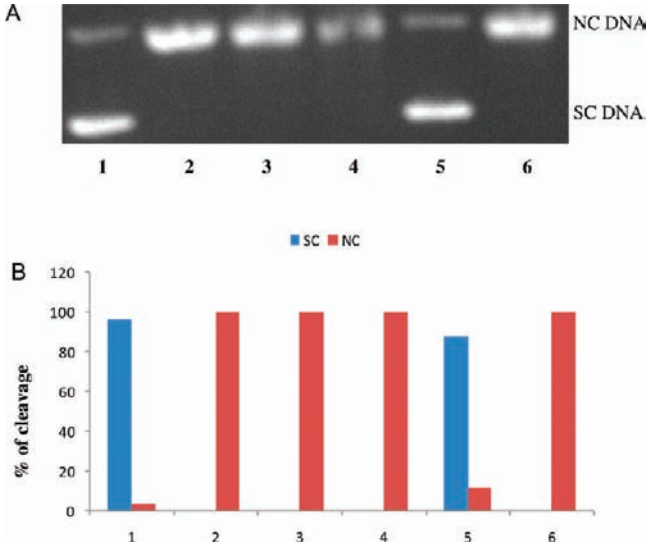

Figure 14. (A) Gel electrophoresis diagram of cleavage of supercoiled pUC19 DNA (40 μM) by the complex **4** (200 μM) in 2% DMF:5 mM Tris-HCl/50 mM NaCl at pH = 7.1 and in the presence of different additives at 37 °C. Lane 1, DNA; lane 2, DNA + **4**; lane 3, DNA + **4** + NaN_3 (100 μM); lane 4, DNA + **4** + SOD (4 unit); lane 5, DNA + **4** + DMSO (6 μL); lane 6, DNA + **4** + catalase (6 unit). Forms SC and NC are supercoiled and nicked circular DNA, respectively. (B) Bar diagram showing the relative amounts of the different DNA forms in the presence of complex **4** and different additives.

double-strand cleavage of DNA more efficient than their bis-complexes $[Cu(dpq)_2]^{2+}$ and $[Cu(phen)_2]^{2+}$ (Figures S7 and S8, Supporting Information). In contrast, **1** and **3** are not effective in cleaving DNA. The intense nuclease activity of **4** is apparently due to enhanced stabilization of the Cu(I) species $[Cu(bba)(dpq)]^+$, as evidenced by its highest Cu(II)/Cu(I)

dx.doi.org/10.1021/ic2017177 | Inorg. Chem. 2012, 51, 5512–5532

redox potential (cf. above). The ability of the dpq co-ligand with extended aromatic ring enables the Cu(I) center generated in the presence of ascorbic acid to be located close to the place of reaction by engaging in strong partial π stacking interaction with DNA. We have shown earlier that for bis(diimine)Cu(II) complexes, the K_+/K_{2+} values vary in the order $[(4\text{-methyl-OP})_2Cu]^{2+}$ > $[(OP)_2Cu]^{2+}$ > $[(5,6\text{-dimethyl-OP})_2Cu]^{2+}$ > $[(5\text{-nitro-OP})_2Cu]^{2+}$ > $[(5\text{-methylOP})_2Cu]^{2+}$ > $[(4,7\text{-dimethyl-OP})_2Cu]^{2+}$ > $[(3,4,7,8\text{-tmphen})_2Cu]^{2+}$ representing the preferential DNA interaction of the bis-complexes in copper(I) form over the copper(II) form. Karmakar et al. have used[86] fluorescence measurements to show that the Cu(I) form of the complex $[Cu(mal)_2](picH)\cdot 2H_2O$ possesses DNA binding affinity (K_b, 6.94×10^4 M^{-1}) higher than the Cu(II) form (K_b, 4.00×10^3 M^{-1}). Also, Ivanov et al. have used thermal melting temperature and CD spectroscopic studies to find that Cu(I) has a higher DNA binding affinity than Cu(II) for $CuCl_2$. The thermal stability of the double-stranded DNA helix is enhanced by Cu(I) rather than Cu(II), as indicated by the increase in melting temperature (T_m). So, it is obvious that strong DNA binding through partial π-stacking interaction is an important factor for efficient DNA cleavage. As discussed above, the phen ring with fewer aromatic rings in **2** is involved in weaker partial π stacking interaction with DNA base pairs. The incorporation of methyl groups at 5,6 positions on the phen ring in **3**, unlike **2** and **4**, would sterically hinder the π-stacking of phen ring with DNA base pairs. Whereas the lower DNA cleavage activity of the 5,6-dmp complex is consistent with its DNA groove binding, the lowest nuclease activity of the bpy (**1**) complex reveals its binding on the DNA surface. Similar conclusions have been made by us for $[Cu(L\text{-Tyr})(diimine)]^+$.[32] Also, the extent of DNA cleavage varies exponentially with incubation time (Figure S9, Supporting Information). The preliminary mechanism of DNA strand scission by **4** has been investigated in the presence of several additives under inert atmosphere. The results show that $^\bullet OH$ radicals rather than $^1O_2$ or O_2^- or H_2O_2 are involved in the DNA cleavage reaction (Supporting Information). Also, addition of distamycin fails to inhibit the cleavage of DNA by **1**–**4** suggesting that all the complexes prefer to bind in the DNA major groove.

DNA Cleavage with Hydrogen Peroxide Added as Reductant. The ability of **1**–**4** to cause DNA cleavage was studied in the presence of H_2O_2 also. At 10 μM complex concentration both **2** and **3** convert SC form to NC and LC forms, while **1** and **4** cause poor DNA cleavage (Figure S10, Table S11, Supporting Information). In the control experiments with DNA alone and DNA with H_2O_2 alone no DNA cleavage is observed. As concentrations of **2** and **3** are increased, the amount of form I decreases and those of both forms II and III increase. At lower complex concentrations, **3** (5 μM) and **2** (10 μM) exhibit maximum double-stand DNA cleavage (Figures S11A,B and S12, Tables S12 and S13, Supporting Information). Interestingly, even at 5 μM concentration **3** displays the same percentage of DNA cleavage as **2** (Figures S12, Table S12, Supporting Information), and at 15 μM complex concentration smaller fragments of undetectable DNA are observed (Supporting Information). In the presence of H_2O_2 as a reducing agent, Cu(II) species are reduced to Cu(I) species which binds to DNA with affinity higher than Cu(II) species,[86] and thus DNA is made more accessible for the reactive oxygen species ($^\bullet OH$) produced by the Fenton type reaction (Figure S14, Scheme 2), resulting in DNA cleavage. The mechanistic studies on DNA cleavage

Scheme 2. Proposed Mechanism for DNA Cleavage by Copper(II) Complexes in the Presence of H_2O_2

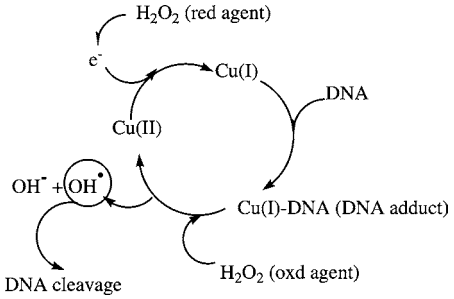

show that $^\bullet OH$ radicals are involved in DNA cleavage reaction (Supporting Information). Also, addition of distamycin does not inhibit the ability of **1**–**4** to cleave DNA suggesting that all the complexes prefer to bind in the DNA major groove.

In both cases, the reduction of DNA bound Cu(II) complex to Cu(I) occurs and hydroxyl radicals are generated. However, in the ascorbic acid mechanism proposed already,[37] dissolved oxygen is needed, whereas in H_2O_2 reaction, H_2O_2 is needed for both reduction and oxidation steps. Thus the difference in the mode of DNA binding of the complexes and the availability of dissolved oxygen or H_2O_2, determine the DNA cleavage ability, which are different for dpq and dmp complexes. So, obviously, the DNA groove bound complex **3** acquires DNA cleavage ability higher than the partially intercalating complex **4** as H_2O_2 is available in higher concentration to **3**. On the other hand, the strongly DNA bound complex **4** located near the cleavage site is stabilized more in the Cu(I) state and so shows higher DNA cleavage by using dissolved oxygen.

DNA Linearization in the Presence of Added Reductants. As complexes **2**–**4** produce a well-defined electrophoresis band characteristic of the LC form, their ability to mediate the cleavage reaction at nicked sites to produce proximate cuts on the complementary strand to generate the LC form was studied. In order to assess whether the observed linearization truly represents a nonrandom linearization process, the statistical test of Povirk et al. that was used to assay double-strand DNA cleavage by bleomycin[63,89] and calicheamicin[90] was applied. Thus, the concentrations of complexes (5 μM) and the activating agents ascorbic acid/hydrogen peroxide (5 μM) are balanced to form LC DNA with supercoiled DNA still remaining so that the required fractions of DNA can be obtained (Figure 15) and the statistical results of DNA linearization experiments were performed under a variety of reaction conditions. The values of n_1/n_2 (n_1 and n_2 are the numbers of single-strand breaks and double-strand breaks, respectively) obtained (0.6–12.5, Table 8) reveal that double-strand rather than single-strand breaks lead to the formation of linear DNA. Also, for the maximum n_1 value, the Freifelder-Trumbo relationship suggests that approximately 120 ssb's are required to effect one dsb ($n_1/n_2 \ll 120$) so as to render the cleavage process nonrandom. Thus it is evident that under all the reaction conditions studied, both in the presence of ascorbic acid and hydrogen peroxide, a nonrandom DNA cleavage process is suggested for **2**–**4**.

Thus, only complex **4**, which exhibits the highest DNA binding affinity and the highest Cu(II)/Cu(I) redox potential,

dx.doi.org/10.1021/ic2017177 | Inorg. Chem. 2012, 51, 5512–5532

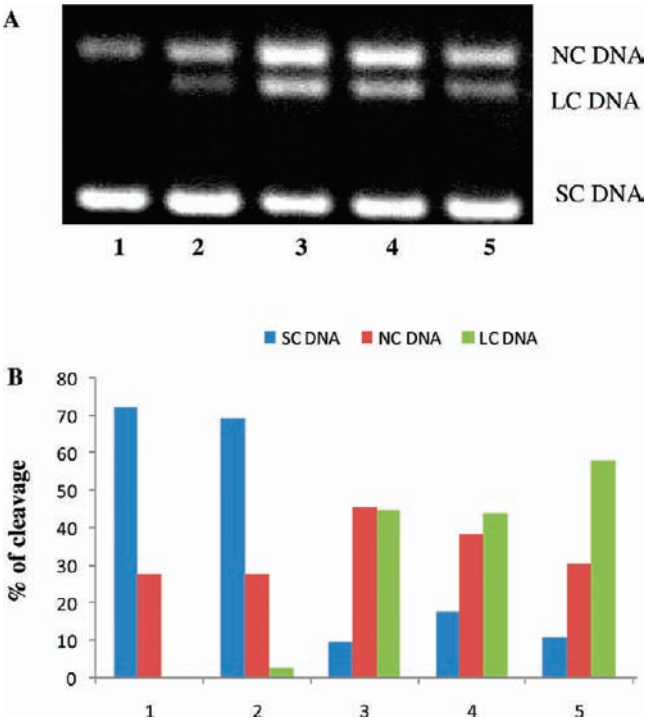

Figure 15. Cleavage of supercoiled pUC19 DNA (40 μM) by complexes **2**–**4** (5 μM) in a buffer containing 2% DMF:5 mM Tris HCl and 50 mM NaCl at pH = 7.1 in the presence of ascorbic acid (H_2A, 5 μM)/hydrogen peroxide (H_2O_2, 5 μM) and 37 °C with an incubation time of 1 h. Lane 1, DNA; lane 2, DNA + H_2A + **2**; lane 3, DNA + H_2A + **4**; lane 4, DNA + H_2O_2 + **2**; lane 5, DNA + H_2O_2 + **3**. Forms SC and NC are supercoiled and nicked circular DNA, respectively. (B) Bar diagram showing the relative amounts of the different DNA forms in the presence of complexes **2**–**4** in the presence of ascorbic acid (H_2A, 5 μM)/hydrogen peroxide (H_2O_2, 5 μM).

Table 8. Investigation of DNA Linearization: Cleavage Data of SC pUC19 DNA (40 μM in Base Pair) by Complexes 2–4 (5 μM) in the Presence of Ascorbic Acid (H_2A, 5 μM)/ Hydrogen Peroxide (H_2O_2, 5 μM) for Incubation Time of 1 h

		form (%)					
S. no.	reaction conditions	SC	NC	LC	n_1	n_2	n_1/n_2
1	DNA control	72.3	27.7				
2	DNA + H_2A + **2** (5 μM)	69.4	27.9	2.7	0.338	0.027	12.51
3	DNA + H_2A + **4** (5 μM)	9.6	45.5	44.8	1.532	0.811	1.89
4	DNA + H_2O_2 + **2** (5 μM)	17.7	38.2	44.2	0.939	0.792	1.19
5	DNA + H_2O_2 + **3** (5 μM)	11.0	30.9	58.1	0.821	1.386	0.59

cleaves DNA even in the absence of an added reductant. The partially intercalating complexes **4** and **2** exhibit more efficient DNA cleavage in the presence of ascorbic acid. Upon DNA binding **4** and **2** with higher Cu(II)/Cu(I) redox potentials undergo reduction to their Cu(I) forms, which are involved in DNA cleavage. In contrast, both **3** and **1**, respectively, bound to the DNA groove and DNA surface, generate •OH radicals when exposed to H_2O_2 and cleave DNA more efficiently than **2** and **4**. Interesting, the 5,6-dmp complex **3** is more effective in generating ROS species in cancer cells and acts as an anticancer agent (cf. below).

Protein Binding and Cleavage Studies. To investigate the interaction of **1**–**4** with proteins, tryptophan emission-quenching experiments were carried out using BSA. It is known that the emission intensity of BSA depends on the degree of exposure of the two tryptophan side chains[91] 134 and 212 to polar solvents and also on the proximity of BSA to specific quenching groups such as protonated carbonyl, protonated imidazole, deprotonated ε-amino groups, and tyrosinate anions.[92] Upon addition of **1**–**4**, the emission intensity of BSA is found to decrease revealing that changes in the protein secondary structure as well as the tryptophan environment of BSA occur upon binding of the complexes.[65] The extent of quenching of fluorescence intensity, as expressed by the value of Stern–Volmer constant (K_{sv}) is a measure of protein binding affinity of the complexes.[93] The value of K_{sv} obtained as slope of the linear plot of I/I_0 vs [complex] follows the order **3** > **4** > **2** > **1** (Figure 16A,B, Table 6). The higher protein-binding

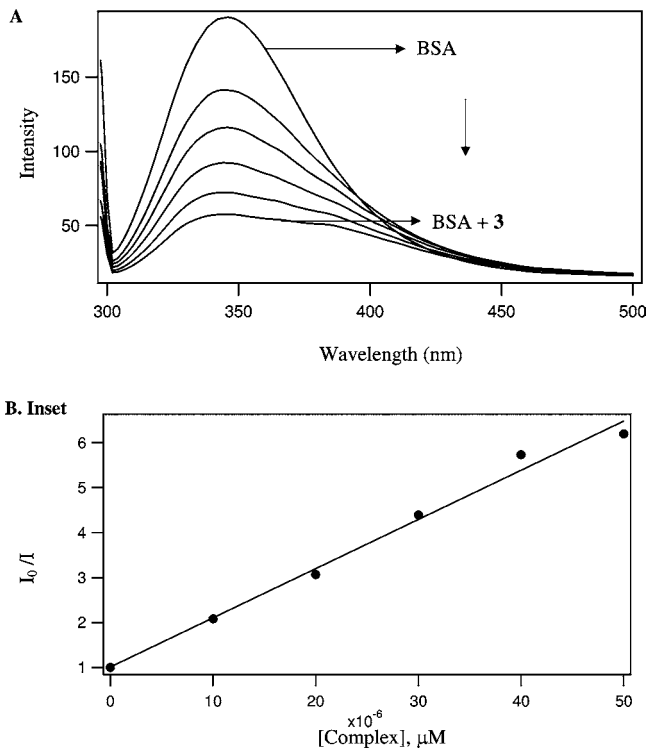

Figure 16. (A) Fluorescence quenching of BSA in the absence and presence of **3** in a phosphate buffer at pH 7.1. Excitation wavelength 295 nm. (B) The plot of I_0/I vs [complex].

affinity of **3** is due to enhanced hydrophobicity of the 5,6-dmp ligand.

The ability of **1**–**4** to cleave protein peptide bonds was studied using BSA. In the absence of an activator like ascorbic acid and hydrogen peroxide, no site specific protein cleavage is observed (Figure S14, Supporting Information). When the protein (4 μM) was incubated at 50 °C (Figure S15, Supporting Information) with **1**–**4** (500 μM) in the presence of H_2O_2 (500 μM) at pH 7.2 and then subjected to SDS–PAGE,[94] all the complexes show protein cleavage compared with the untreated BSA control band and BSA molecular weight marker band. All the complexes show smearing or fading of the BSA band suggesting that the nonspecific binding of the complexes to BSA causes the cleavage of BSA into very small fragments. This is in contrast to the site-specific protein cleavage observed for the $[Cu(tdp)(tmp)]^{2+}$ complex.[31] The

dx.doi.org/10.1021/ic2017177 | Inorg. Chem. 2012, 51, 5512–5532

ability of the complexes to affect protein cleavage follows the order **3** > **4** > **2** > **1**. The highest protein cleavage ability of **3** is due to the hydrophobic methyl substituents of coordinated 5,6-dmp co-ligand, which recognize the more exposed hydrophobic regions of the protein and facilitate the protein cleavage. Further cleavage experiments were conducted by varying the concentration of **2**–**4** (100–500 μM) and keeping that of BSA constant. The complex **3** is found to exhibit efficient BSA cleavage even at 100 μM concentration (Figure 17), whereas **2**

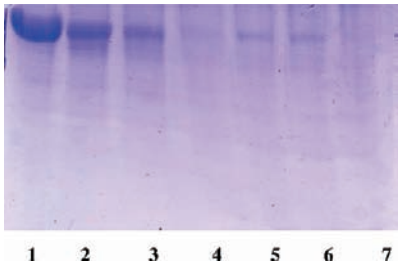

Figure 17. SDS–PAGE diagram of cleavage of bovine serum albumin (BSA, 4 μM) using various concentrations of complex **3** in a 2% DMF:5 mM Tris-HCl/50 mM NaCl at pH = 7.1 and in the presence of hydrogen peroxide (H_2O_2, 500 μM) at 50 °C for 3 h. Lane 1, BSA; lane 2, BSA + H_2O_2; lane 3, BSA + H_2O_2 + **3** (100 μM); lane 4, BSA + H_2O_2 + **3** (200 μM); lane 5, BSA + H_2O_2 + **3** (300 μM); lane 6, BSA + H_2O_2 + **3** (400 μM); lane 7, BSA + H_2O_2 + **3** (500 μM).

and **4** also show efficient BSA cleavage but at higher concentrations of 300 and 200 μM, respectively (Figures S16 and 17, Supporting Information). MALDI-TOF MS analysis of BSA (4 μM) was performed in the absence and presence of **3** (100 μM) after incubation with H_2O_2 for 3 h. In the absence of **3** a significantly intense peak with the m/z value (65875.8) corresponding to uncleaved BSA and also two less intense peaks with m/z (33066.8, 22039.9) corresponding to cleavage mainly occurring at spontaneous cleavage sites (possibly Asp residues)[95] in BSA (Figure 18A) are observed. When BSA was incubated with **3** no measurable peak intensity is observed in the mass spectrum (Figure 18B) revealing complete degradation of the protein by **3**. When the hydroxyl radical scavenger DMSO is added to the reaction mixture, inhibition of BSA cleavage is observed revealing the involvement of $^{\bullet}$OH radicals in the cleavage reaction (Figure S18, Supporting Information). Interestingly, the same complex binds to the DNA grooves more strongly than other complexes and generates ROS species more efficiently. This suggests that the hydrophobicity of the complex plays a significant role in DNA and protein binding.

Anticancer Activity Studies. *MTT Assay.* The anticancer activity of **1**–**4** against cervical cancer cell lines (SiHa) has been investigated in comparison with the widely used drug cisplatin under identical conditions by using the MTT assay. The IC_{50} values for 48 h incubation are lower than those for 24 h incubation, clearly indicating that the cytotoxicities are time dependent. The ability of the complexes to kill the cancer cells vary as **3** > **4** > **2** > **1** and, interestingly, **3** and **4** exhibit higher cytotoxicity than cisplatin for both 24 and 48 h incubations (Table 9). The high cytotoxicity of **3** may originate from the strong hydrophobic forces of interaction of the complex with both DNA and protein. A similar correlation has been

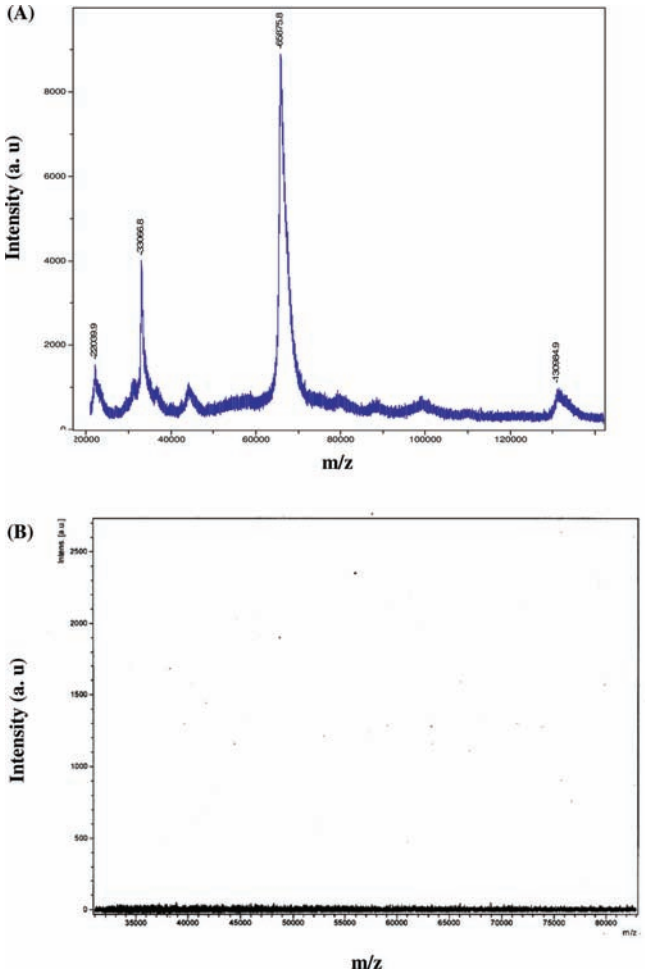

Figure 18. MALDI-TOF MS spectra of cleavage of bovine serum albumin (BSA, 4 μM) by complex **3** (100 μM) in 2% DMF:5 mM Tris-HCl/50 mM NaCl buffer at pH = 7.1 and in the presence of hydrogen peroxide (H_2O_2, 500 μM) and at 50 °C with an incubation time of 3 h. (A) BSA + H_2O_2; (B) BSA + H_2O_2 + **3**.

Table 9. In Vitro Cytotoxicity Assays for Complexes 1–4 against Cervical Cancer Cell Line (SiHa)[a]

	inhibitory concentration (IC_{50}, μM)	
complexes	24 h	48 h
$[Cu(bba)(bpy)]^{2+}$ (**1**)	18.0 ± 1.3	13.2 ± 1.2
$[Cu(bba)(phen)]^{2+}$ (**2**)	7.3 ± 0.2	3.1 ± 0.3
$[Cu(bba)(5,6\text{-dmp})]^{2+}$ (**3**)	3.2 ± 0.3	0.9 ± 0.2
$[Cu(bba)(dpq)]^{2+}$ (**4**)	5.2 ± 0.4	2.1 ± 0.3
cisplatin	6.7 ± 0.2	5.0 ± 0.3

[a]Data are mean ± SD of three replicates each.

observed for the mixed-ligand complexes $[Cu(tdp)(tmp)]^{+}$,[31] $[Cu(L\text{-tyr})(5,6\text{-dmp})]^{+}$,[32] and $[Cu_2(LH)_2(5,6\text{-dmp})_2(ClO_4)_2]^{2+}$,[47] which exhibit DNA binding affinity higher than those of their bpy, phen, and dpq analogues due to strong hydrophobic forces of interaction involving tmp and 5,6-dmp coligands. Also, the enhanced hydrophobicity of 5,6-dmp coligand facilitates the transport of **3** into the cell across cell membrane. Further, the adherence of the positively charged metal complexes to the plasma membrane by electrostatic attraction before its transport across the membrane

dx.doi.org/10.1021/ic2017177 | *Inorg. Chem.* 2012, 51, 5512–5532

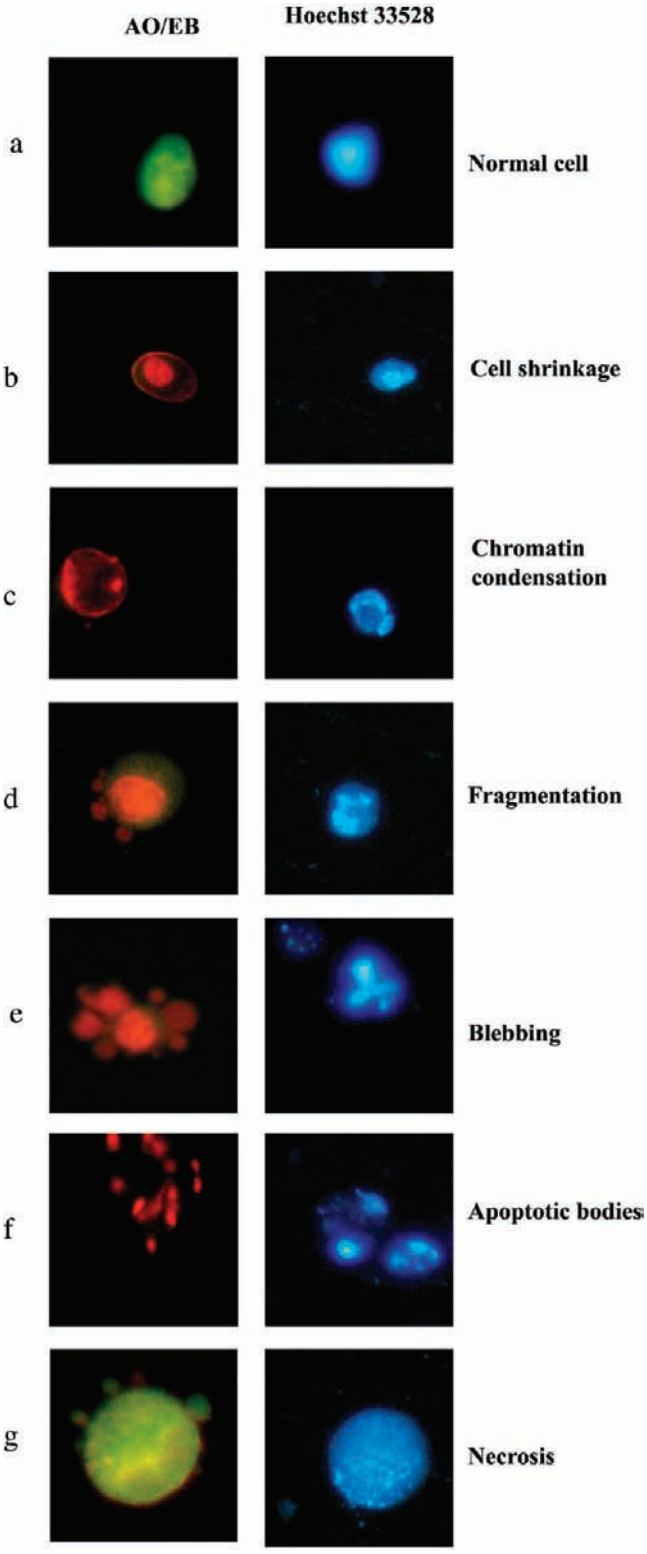

Figure 19. Representative morphological changes observed for complex **3** by adopting Hoechst 33258 staining and AO/EB staining against SiHa human cervical cells. (a) Normal cells, (b–g) treated with complex **3** at 48 h incubation.

is facilitated by the difference in concentration gradient of the complex.[31,32,47]

Hoechst Staining Studies. As a distinct series of cellular pathways, apoptosis potentially offers unique targets for chemotherapeutic intervention. It has been suggested that

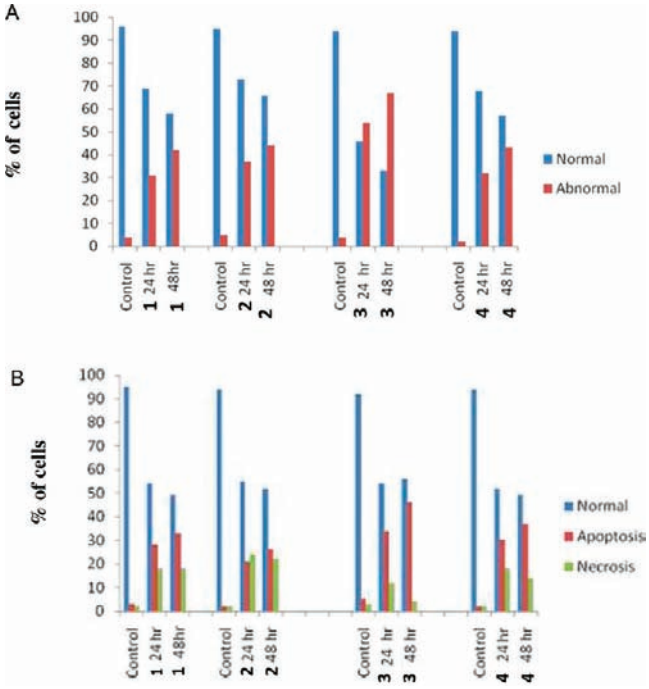

Figure 20. (A) Hoechst 33258 staining study of **1**–**4** induced apoptosis of SiHa human cervical cancer cells. Graph shown manual count of apoptotic cells in percentage (Data are mean% ± SD% of each triplicate). (B) AO/EB fluorescent study of **3** induced apoptosis of SiHa human cervical cells. Graph shown manual count of apoptotic cells in percentage (Data are mean% ± SD% of each triplicate).

cancer cells are more sensitive to several apoptosis-inducing stimuli than normal cells, including proteasome inhibitors and those affecting cellular division.[96] The molecular mechanism of cell death has been studied by treating the SiHa cancer cells with IC_{50} concentrations of **1**–**4** for 24 h and 48 h and then observing them for cytological changes by adopting Hoechst 33258 staining (Figures 19 and 20A). For all the complexes apoptosis is found to occur in a well-choreographed sequence of morphological events. The dying cell thus undergoes nuclear and cytoplasmic condensation with blebbing of the plasma membrane, and eventually breaks up into membrane-enclosed particles termed apoptotic bodies containing intact organelles, as well as portions of the nucleus. These apoptotic bodies are then rapidly recognized, ingested and degraded by professional phagocytes and neighboring cells. The representative morphological changes observed for **3** such as chromatin fragmentation, bi- and/or multinucleation, cytoplasmic vacuolation, nuclear swelling, cytoplasmic blebbing and late apoptosis indication of dot-like chromatin condensation are shown in Figure 19. Also, the number of abnormal cells is found to increase with incubation time revealing that all the complexes bring about cytological changes in a time dependent manner (Figure 20A). Further, the number of abnormal cells generated at both 24 and 48 h varies as **3** > **4** > **2** > **1** (Figure 20A). The higher apoptosis-inducing ability of **3** is consistent with the hydrophobic 5, 6-dmp co-ligands, which facilitate transport of the complex across the cell membrane and its eventual release at various organells in the cell leading to apoptosis. Similar observations have been made by us for the mixed ligand complexes $[Cu(tdp)(tmp)]^+$,[31] $[Cu(L\text{-}tyr)(5,6\text{-}dmp)]^+$,[32]

dx.doi.org/10.1021/ic2017177 | *Inorg. Chem.* 2012, 51, 5512–5532

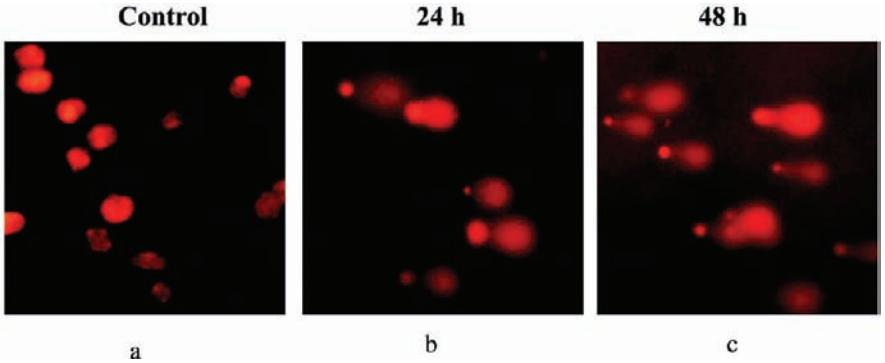

Figure 21. Comet assay of EB-stained SiHa human cervical cancer cells. (a) normal cells (untreated), (b) treated with complex **3** at 24 h incubation, (c) at 48 h incubation.

and $[Cu_2(LH)_2(5,6\text{-dmp})_2(ClO_4)_2]^{2+}$.[47] As the apoptosis-inducing ability is critical in determining the efficacy of an anticancer drug, the complex **3** with a higher apoptosis-inducing ability is obviously more efficacious than **4**.

AO/EB Staining Studies. The apoptotic morphologies induced by **1**−**4** are confirmed by using AO/EB staining and adopting fluorescence microscopy (Figures 19 and 20B). The cytological changes observed are classified[68] into four types according to the fluorescence emission and morphological features of chromatin condensation in the AO/EB stained nuclei: (i) viable cells having uniformly green fluorescing nuclei with highly organized structure; (ii) early apoptotic cells (which still have intact membranes but have started undergoing DNA fragmentation) having green fluorescing nuclei, but perinuclear chromatin condensation is visible as bright green patches or fragments; (iii) late apoptotic cells having orange to red fluorescing nuclei with condensed or fragmented chromatin; and (iv) necrotic cells, swollen to large sizes, having uniformly orange to red fluorescing nuclei with no indication of chromatin fragmentation. The morphological changes observed for **1**−**4** suggest that the cells are committed to death in such a way that both apoptotic and necrotic cells increase in number in a time-dependent manner. The ability of the complexes to induce apoptotic cell death follows the order **3** > **4** > **1** > **2**, with both **3** and **4** causing more cells to take to preferentially one particular mode of cell death (apoptosis) during 48 h treatment than during 24 h treatment, which is in line with the results from Hoechst staining.

Comet Assay. DNA fragmentation, which is a hallmark of apoptosis, is detected at a single cell level by the use of single cell gel electrophoresis (comet assay) in agarose gel matrix. When a cell with damaged DNA is subjected to electrophoresis and then stained with EB, it appears as a comet. Cells treated with **3** shows statistically significant and well-formed comets, whereas the control (untreated) cells do not demonstrate any such comet like appearance (Figure 21). Also, the longer tail length observed for **3** is consistent with its highest cytotoxicity (cf. above) as the length of the comet tail is a measure of extent of DNA damage.[97] This clearly indicates that **3** indeed induces DNA fragmentation, which is a further evidence for its ability to induce higher apoptosis.

Intracellular ROS Generation. ROS have been suggested as possible mediators of apoptosis induced by copper(II) complexes by oxidative stress.[71] The ability of **1**−**4** to produce ROS in SiHa cells was examined by using the fluorescent probe DCFH-DA. After the cancer cells were treated for 12 h with the complexes, an increase in intracellular ROS, as measured by the increase in fluorescence intensity of DCF, is observed for all the complexes in comparison with the control (Figure 22A,B). The amount of intracellular ROS species generated by the copper(II) complexes follows the order **3** > **4** > **2** > **1**, which is the same as that observed for IC_{50} values. This reveals that the complexes function as anticancer agents by strongly binding to DNA and generating ROS species. Thus **3**, which exhibits significant DNA binding affinity and affects double-strand DNA cleavage, activates the ROS-generating machinery and generates the highest amount of ROS when treated with cancer cells, leading to apoptosis. Thus, it is clear that the complex acts as an efficient anticancer agent by oxidative stress.

The complexes are thought to be bound to the plasma proteins, transported through biological fluids and then eventually released at the cellular level to exhibit anticancer activity.[95] Thus the strongest protein binding affinity of **3** (cf. above), apart from its stongest DNA binding affinity, may be responsible for its highest cytotoxicity. However, upon their binding to proteins the complexes might lead to drastic modifications, or even loss, of their biological properties. We have made similar conclusions earlier for mixed-ligand Cu(II) complexes containing 5,6-dmp co-ligand.[31,32,47] Very recently, the anticancer activity of certain Ru(III) complexes has been related[95] to their ability to bind to proteins and cause severe inhibition of some fundamental enzyme function.

All the above discussions clearly reveal that the prominent cytotoxicity of **3** is consistent with its strong protein and DNA binding affinity and its higher ability to affect double-stranded DNA cleavage under physiological conditions and hence kill the cancer cells. Also, the enhanced hydrophobicity of the complex facilitates its transport into the cell (cf. above) so as to interfere with the cellular function of DNA. As the copper(II) complexes of polybenzimidazole ligands are known to affect condensation of free DNA,[98] and facilitate intracellular trafficking into the nuclei, we propose that the bzim moieties of the present copper(II) complexes enhance the DNA binding affinity through hydrophobic interaction (cf above). Such observations help us in identifying additional molecular targets for the development of transition metal-based chemotherapeutic agents. Also, additional biochemical experiments like cell cycle analysis are to be performed to confirm the modes of cell death observed for the complexes.

dx.doi.org/10.1021/ic2017177 | *Inorg. Chem.* 2012, 51, 5512−5532

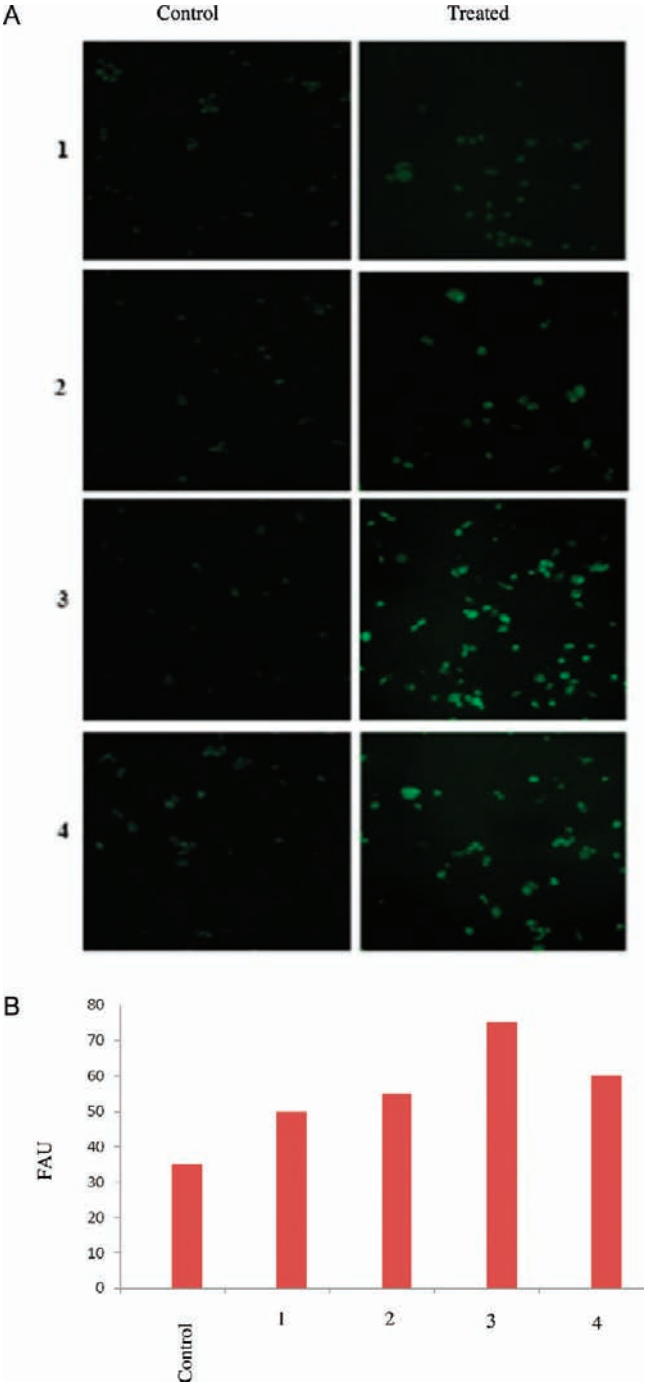

Figure 22. (A) SiHa cells showing an increase in the ROS level when treated with complexes **1**−**4**. Left panels are untreated controls. Right panels correspond to the treated with complexes **1**−**4** (12 h). ROS generation was studied using dichlorofluorescin diacetate (DCFH-DA) dye assay. (B) SiHa cells showing an increase in the ROS level when treated with compounds **1**−**4** . The relative levels of fluorescence were quantified by fluorescence spectrometry (FAU: fluorescence arbitrary units). ROS generation was studied using dichlorofluorescin diacetate (DCFH-DA) dye.

CONCLUSIONS

In the mixed-ligand complexes $[Cu(bba)(diimine)]^{2+}$, where diimine is bpy or 5,6-dmp or dpq, the tridentate ligand bba is meridionally coordinated to Cu(II) while it is facially coordinated in $[Cu(bba)(phen)]^{2+}$. However, interestingly, all the complexes possess meridional coordination of bba in solution. The phen and dpq co-ligands are involved in π-stacking interaction with DNA base pairs, while the 5,6-dmp and bpy co-ligands are involved in respectively hydrophobic and electrostatic interactions with DNA. Thus the diimine co-ligands, which could function as a DNA recognition element, dictate the DNA binding affinity of the mixed ligand Cu(II) complexes. The dpq complex is unique in displaying prominent DNA cleavage even in the absence of an activator and also exhibits oxidative (ascorbic acid) double-strand DNA cleavage with efficiency more profound and prominent than its 5,6-dmp, phen, and bpy analogues. Interestingly, even at 10 μM concentration, the 5,6-dmp complex effects double-strand DNA cleavage in the presence of H_2O_2 as an activator with efficiency higher than its bpy, phen and dpq analogues. So, it is suggested that dpq and 5,6-dmp co-ligands could be incorporated as DNA recognition elements in designing robust and efficient copper(II)-based chemical nucleases.

The 5,6-dmp complex is remarkable in displaying cytotoxicity against SiHa cervical cancer cell lines more potent than its dpq, phen, and bpy analogues, which is consistent with its strong ability to bind with DNA as well as cellular proteins and also cleave it by double-strand scission. The prominent cytotoxicity is traced to the hydrophobicity of the complex conferred upon it by the 5,6-dmp co-ligand. Also, the complex is a promising drug for potential clinical applications in cancer therapy as it damages DNA by double-strand cleavage and causes cell death mainly through apoptotic mode. Thus, suitable hydrophobic co-ligands such as 5,6-dmp may be incorporated as DNA recognition elements in designing efficient metal-based anticancer agents.

ASSOCIATED CONTENT

Supporting Information

Crystallographic information files. Results and discussion of the ethidium bromide displacement assay, viscosity measurements, DNA cleavage studies, and protein cleavage studies; additional tables and figures as described in the text. This material is available free of charge via the Internet at http://pubs.acs.org.

AUTHOR INFORMATION

Corresponding Author

*E-mail: palaniandavarm@gmail.com, palanim51@yahoo.com.

Present Addresses

[⊥]Visiting Professor, Department of Food Sciences and Nutrition, College of Food Sciences and Agriculture, King Saud University, Riyadh-11451, Kingdom of Saudi Arabia.

[#]Visiting Fellow, Central University of Tamil Nadu, Thiruvarur 610001, India.

Notes

The authors declare no competing financial interest.

ACKNOWLEDGMENTS

M.P. is a recipient of Ramanna National Fellowship of Department of Science and Technology, New Delhi. DST Ramanna Fellowship (Grant Nos. SR/S1/RFIC/01/2007-2010 and SR/S1/RFIC/01/2010-2013) is acknowledged for a Junior Research Fellowship to R.L. The X-ray diffraction facility in the Department was created by funding from Department of Science and Technology (DST-FIST), New Delhi, and EPR and fluorescence spectral facilities were created by University Grants Commission (SAP), New Delhi. We thank Professor

P.R. Athappan, Madurai Kamaraj University, Madurai, for providing the CD facilities, Dr. Balachandran Unni Nair, CLRI, for providing the ESI−MS facilities, and Professor P. Sambasiva Rao, Pondicherry University, for providing EPR facilities. We thank Prof. S. Manogaran, Department of Chemistry, Indian Institute of Technology Kanpur, for helping with the solvent phase DFT calculations. We thank Mr. R. Padmanaban, System Administrator, Bharathidasan University Informatics Centre for help in DFT calculations.

REFERENCES

(1) Giaccone, G.; Herbst, R. S.; Manegold, C.; Scagliotti, G.; Rosell, R.; Miller, V. *J. Clin. Oncol.* **2004**, *22*, 777−784.
(2) Maheswari, P. U.; Roy, S.; Dulk, H. D.; Barends, S.; Wezel, G. V.; Kozlevcar, B.; Gamez, P.; Reedijk, J. *J. Am. Chem. Soc.* **2006**, *128*, 710−711.
(3) Ranford, J. D.; Sadler, P. J.; Tocher, D. A. *J. Chem. Soc., Dalton Trans.* **1993**, 3393−3399.
(4) Ng, C. H.; Kong, K. C.; Von, S. T.; Balraj, P.; Jensen, P.; Thirthagiri, E.; Hamada, H.; Chikira, M. *Dalton Trans.* **2008**, 447−454.
(5) Barve, A.; Kumbhar, A.; Bhat, M.; Joshi, B.; Butcher, R.; Sonawane, U.; Joshi, R. *Inorg. Chem.* **2009**, *48*, 9120−9132.
(6) (a) Hotze, A. C. G.; Caspers, S. E.; de Vos, D.; Kooijman, H.; Spek, A. L.; Flamigni, A.; Bacac, M.; Sava, G.; Haasnoot, J. G.; Reedijk, J. *J. Biol. Inorg. Chem.* **2004**, *9*, 354. (b) Hotze, A. C. G.; Kariuki, B. M.; Hannon, M. J. *Angew. Chem., Int. Ed.* **2006**, *45*, 4839.
(7) (a) Hartinger, C. G.; Zorbas-Seifried, S.; Jakupec, M. A.; Kynast, B.; Zorbas, H.; Keppler, B. K. *J. Inorg. Biochem.* **2006**, *100*, 891. (b) Galanski, M.; Arion, V. B.; Jakupee, M. A.; Keppler, B. K. *Curr. Pharm. Des.* **2003**, *9*, 2078.
(8) (a) Fuertes, M. A.; Alonso, C.; Perez, M. J. *Chem. Rev.* **2003**, *103*, 645. (b) Clarke, M. J.; Zhu, F. C.; Frasca, D. R. *Chem. Rev.* **1999**, *99*, 2511.
(9) (a) Cocchietto, M.; Sava, G. *Pharmacol. Toxicol.* **2000**, *87*, 193. (b) Zorzet, S.; Sorc, A.; Casarsa, C.; Cocchietto, M.; Sava, G. *Met.-Based Drugs* **2001**, *8*, 1. (c) Gagliardi, R.; Sava, G.; Pacor, S.; Mestroni, V.; Alessio, E. *Clin. Exp. Metastasis* **1994**, *12*, 93. (d) Magnarin, M.; Bergamo, A.; Carotenuto, M. E.; Zorzet, S.; Sava, G. *Anticancer Res.* **2000**, *20*, 2939. (e) Rademaker-Lakhai, J. M.; Van den Bongard, D.; Pluim, D.; Beijnen, J. H.; Schellens, J. H. *Clin. Cancer Res.* **2004**, *10*, 3717.
(10) (a) Sava, G.; Clerici, K.; Capozzi, I.; Cocchietto, M.; Gagliardi, R.; Alessio, E.; Mestroni, G. *Anti-Cancer Drugs* **1999**, *10*, 129. (b) Sava, G.; Gagliardi, R.; Bergamo, A.; Alessio, E.; Mestroni, G. *Anticancer Res.* **1999**, *19*, 969. (c) Sava, G.; Gagliardi, R.; Cocchietto, M.; Clerici, K.; Capozzi, I.; Marella, M.; Alessio, E.; Mestroni, G.; Milanino, R. *Pathol. Oncol. Res.* **1998**, *4*, 30.
(11) (a) Keppler, B. K.; Henn, M.; Juhl, U. M.; Berger, M. R.; Niebl, R.; Wagner, F. E. *Prog. Clin. Biochem. Med.* **1989**, *10*, 41. (b) Kreuser, E. D.; Keppler, B. K.; Berdel, W. E.; Piest, A.; Thiel, E. *Semin. Oncol.* **1992**, *19*, 73.
(12) (a) Morris, R. E.; Aird, R. E.; Murdoch, P. D.; Chen, H. M.; Cummings, J.; Hughes, N. D.; Parsons, S.; Parkin, A.; Boyd, G.; Jodrell, D. I.; Sadler, P. J. *J. Med. Chem.* **2001**, *44*, 3616. (b) Yan, K. Y.; Melchart, V; Habtemariam, A.; Sadler, P. J. *Chem. Commun.* **2005**, 4764. (c) Novakova, O.; Chen, H.; Vrana, M. O.; Rodger, A.; Sadler, P. J.; Brabec, V. *Biochemistry* **2003**, *42*, 11544.
(13) Fernandes, C.; Parrilha, G. L.; Lessa, J. A.; Santiago, L. J. M.; Kanashiro, M. M.; Boniolo, F. S.; Bortoluzzi, A. J.; Vugman, N. V.; Herbstand, M. H.; H., A., Jr. *Inorg. Chim. Acta* **2006**, *359*, 3167.
(14) Bales, B. C.; Kodama, T.; Weledji, Y. N.; Pitie, M.; Meunier, B.; Greenberg, M. M. *Nucleic Acids Res.* **2005**, *33*, 5371.
(15) Kraatz, H. B.; Metzler-Nolte, N. *Concepts and Models in Bioinorganic Chemistry*; WILEY-VCH: Weinheim, Germany, 2006; p 365.
(16) Lippard, S. J.; Berg, J. M. *Principles of Bioinorganic Chemistry*; University Science Books: Mill Valley, CA, 1994.
(17) Harris, Z. H.; Gitlin, J. D. *Am. J. Clin. Nutr.* **1996**, *63*, 836S−841S.
(18) Frausto da Silva, J. J. R.; Williams, R. J. P. *The Biological Chemistry of the Elements*; Clarendon: Oxford, U. K., 1991.
(19) Coates, R. J.; Weiss, N. S.; Daling, J. R.; Rettmer, R. L.; Warnick, G. R. *Cancer Res.* **1989**, *49*, 4353−4356.
(20) Gupta, S. K.; Shukla, V. K.; Vaidya, M. P.; Roy, S. K. *J. Surg. Oncol.* **1993**, *52*, 172−175.
(21) Gupta, S. K.; Shukla, V. K.; Vaidya, M. P.; Roy, S. K.; Gupta, S. *J. Surg. Oncol.* **1991**, *46*, 178−181.
(22) Diez, M.; Cerdà, F. J.; Arroyo, M.; Balibrea, J. L. *Cancer* **1989**, *63*, 726−730.
(23) Turecky, L.; Kalina, P.; Uhlikova, E. *Klin. Wochenschr.* **1984**, *62*, 187−189.
(24) Yoshida, D.; Ikeda, Y.; Nakazawa, S. *J. Neurooncol.* **1993**, *16*, 109−115.
(25) Petering, D. H. *Met. Ions Biol. Syst.* **1980**, *11*, 197−229.
(26) (a) French, F. A.; Blanz, E. J., Jr. *Cancer Res.* **1965**, *25*, 1454−1458. (b) French, F. A.; Blanz, E. J., Jr. *Cancer Res.* **1966**, *26*, 1638−1640.
(27) May, P. M.; Williams, D. R. In *Metal Ions in Biological Systems*; Sigel, H., Ed.; Marcel Dekker: New York, 1981; Vol. *12*, Chapter 7.
(28) May, P. M.; Williams, D. R. In *Metal Ions in Biological Systems*; Sigel, H., Ed.; Marcel Dekker: New York, 1981; Vol. *13*.
(29) Miura, T.; Hori-i, A.; Mototani, H.; Takeuchi, H. *Biochemistry* **1999**, *38*, 11560.
(30) Zhang, S.; Zhu, Y.; Tu, C.; Wei, H.; Yang, Z.; Lin, L.; Ding, J.; Zhang, J.; Guo, Z. *J. Inorg. Biochem.* **2004**, *98*, 2099.
(31) (a) Rajendiran, V.; Karthik, R.; Palaniandavar, M.; Evans, H. S.; Periasamay, V. S.; Akbarsha, M. A.; Srinag, B. S.; Krishnamurthy, H. *Inorg. Chem.* **2007**, *46*, 8208. (b) Rajendiran, V.; Palaniandavar, M.; Swaminathan, P.; Uma, L. *Inorg.Chem. (Commun)* **2007**, *46*, 8208.
(32) Ramakrishnan, S.; Rajendiran, V.; Palaniandavar, M.; Periasamay, V. S.; Akbarsha, M. A.; Srinag, B. S.; Krishnamurthy, H. *Inorg. Chem.* **2009**, *48*, 1309.
(33) (a) Povirk, L. F. In *Molecular Aspects of Anti-Cancer Drug Action*; Neidle, S., Waring, M., Eds.; Verlag-Chemie: Weinheim, Germany, 1983; p 157. (b) Povirk, L. F. *Mutat. Res.* **1991**, *257*, 127.
(34) Natrajan, A.; Hecht, S. M. In *Molecular Aspects of Anticancer Drug-DNA Interactions*; Neidle, S., Waring, M., Eds.; CRC Press: Boca Raton, FL, 1994; Vol. *2*, p 197.
(35) Goldberg, I. H. *Molecular Aspects of Anticancer Drug-DNA Interactions*; Neidle, S.,Waring, M., Eds.; CRC Press: Boca Raton, FL, 1993; Vol. *1*, p 243.
(36) (a) Sigman, D. S.; Graham, D. R.; Aurora, V. D.; Stern, A. M. *J. Biol. Chem.* **1979**, *254*, 12269−12272. (b) Spassky, A.; Sigman, D. S. *Biochemistry* **1985**, *24*, 8050−8056. (c) Sigman, D. S.; Mazumder, A.; Perrin, D. M. *Chem. Rev.* **1993**, *93*, 2295−2316.
(37) Detmer, C. A., III; Pamatong, F. V.; Bocarsly, J. R. *Inorg. Chem.* **1996**, *35*, 6292−6298.
(38) Jin, Y.; Cowan, J. A. *J. Am. Chem. Soc.* **2005**, *127*, 8408−8415.
(39) Maheswari, P. U.; Ster, M. V. D.; Smulders, S.; Barends, S.; Wezel, G. P. V; Massera, C.; Roy, S.; Dulk, H. D.; Gamez, P.; Reedijk, J. *Inorg. Chem.* **2008**, *47*, 9.
(40) (a) Dhar, S.; Senapati, D.; Das, P. K.; Chattopaddhyay, P.; Nethaji, M.; Chakravarty, A. R. *J. Am. Chem. Soc.* **2003**, *125*, 12118−12124. (b) Patra, A. K.; Dhar, S.; Nethaji, M.; Chakravarty, A. R. *Chem. Commun.* **2003**, 1562−1563. (c) Dhar, S.; Senapati, D.; Reddy, P. A. N.; Das, P. K.; Chakravarty, A. R. *Chem. Commun.* **2003**, 2452−2453.
(41) Selvakumar, B.; Rajendiran, V.; Uma Maheswari, P.; Evans, H. S.; Palaniandavar, M. *J. Inorg. Biochem.* **2006**, *100*, 316−330.
(42) (a) Murali, M.; Palaniandavar, M. *Dalton Trans.* **2006**, 730. (b) Murali, M.; Palaniandavar, M. *Polyhedron* **2007**, *26*, 3980.
(43) (a) Tanious, F. A.; Hamelberg, D.; Bailly, C.; Czarny, A.; Boykin, D. W.; Wilson, W. D. *J. Am. Chem. Soc.* **2004**, *126*, 143−153. (b) Liu, C. L.; Yu, S. W.; Li, D. F.; Liao, Z. R.; Sun, X. H.; Xu, H. B. *Inorg. Chem.* **2002**, *41*, 913−922. (c) Vaidyanathan, V. G.; Nair, B. U. *J. Inorg. Biochem.* **2003**, *94*, 121−126. (d) Wahnon, D.; Hynes, R. C.; Chin, J. *J. Chem. Soc. Chem. Commun.* **1994**, 1441.

(44) (a) Pjura, P. E.; Grzeskowiak, K.; Dickerson, R. E. *J. Mol. Biol.* **1987**, *197*, 257. (b) Teng, M. K.; Usman, N.; Frederick, C. A.; Wang, A. H. J. *Nucleic Acid Res.* **1988**, *16*, 2671. (c) Aymami, J.; Nunn, C. M.; Neidle, S. *Nucleic Acid Res.* **1999**, *27*, 2691.
(45) (a) Parkinson, J. A.; Barber, J.; Douglas, K. T.; Rosamond, J.; Sharples, D *Biochemistry* **1990**, *29*, 10181. (b) Fede, A.; Labhardt, A.; Bannwarth, W.; Leupin, W. *Biochemistry* **1991**, *30*, 11377.
(46) (a) Wahnon, D.; Hynes, R. C.; Chin, J. *J. Chem. Soc. Chem. Commun.* **1994**, 1441−1442. (b) Liao, Z. R.; Xiang, D. F.; Li, D. F.; Sheng, F.; Mei, F. S. *Synth. React. Inorg. Met.−Org. Chem.* **2000**, *30*, 683−693.
(47) Ramakrishnan, S.; Shakthipriya, D.; Suresh, E.; Periasamy, V. S.; Akbarsha, M. A.; Palaniandavar, M. *Inorg. Chem.* **2011**, *50*, 6458−6471.
(48) (a) Rajendiran, V.; Murali, M.; Suresh, E.; Sinha, S.; Somasundaram, K.; Palaniandavar, M. *Dalton Trans.* **2008**, 148. (b) Rajendiran, V.; Murali, M.; Suresh, E.; Sinha, S.; Somasundaram, K.; Palaniandavar, M. *Dalton Trans.* **2008**, 2157. (d) Rajendiran, V.; Palaniandavar, M.; Periyasamy, V. S.; Akbarsha, M. A. *J. Inorg. Biochem.* **2010**, *104*, 217.
(49) (a) Ramakrishnan, S.; Suresh, E.; Riyasdeen, A.; Akbarsha, M. A.; Palaniandavar, M. *Dalton Trans.* **2011**, *40*, 3524−3536. (b) Ramakrishnan, S.; Suresh, E.; Riyasdeen, A.; Akbarsha, M. A.; Palaniandavar, M. *Dalton Trans.* **2011**, *40*, 3245−3256.
(50) Dhanalakshmi, T.; Suresh, E.; Palaniandavar, M. *Inorg. Chim. Acta* **2011**, *365*, 143.
(51) Kratz, F. In *Metal Complexes in Cancer Chemotherapy*; Keppler, B. K., Ed.; VCH: Weinheim, Germany, 1993; p 391.
(52) McKeage, M. J. *Drug Safety* **1995**, *13*, 228.
(53) (a) Parker, S. H.; Tong, T.; Bolden, S.; Winko, P. A. *Cancer J. Clin.* **1996**, *46*, 5−27. (b) Ishida, S.; McCormick, F.; Smith-McCune, K.; Hanahan, D. *Cancer Cell* **2010**, *17*, 574−583.
(54) Collins, J. G.; Sleeman, A. D.; Aldrich, J. R.; Greguric, I.; Hambly, T. W. *Inorg. Chem.* **1998**, *37*, 3133.
(55) Parker, V. D. In *Electroanalytical Chemistry*; Bard, A. J., Ed.; Marcel Dekker; New York, 1986; Vol. *14*, p 18.
(56) Merill, C.; Goldman, D.; Sedman, S. A.; Ebert, M. H. *Science* **1980**, *211*, 1437−1438.
(57) *SMART & SAINT* Software References manuals, version 5.0; Bruker AXS Inc.: Madison, WI, 1998.
(58) Sheldrick, G. M. *SAINT 5.1*; Siemens Industrial Automation Inc.: Madison, WI, 1995, .
(59) *SADABS, Empirical Absorption Correction Program*; University of Göttingen: Göttingen, Germany, 1997.
(60) (a) Sheldrick, G. M. *SHELXTL Reference Manual*, Version 5.1; Bruker AXS: Madison, WI, 1997. (b) Sheldrick, G. M. *SHELXS-97: Program for the Solution of Crystal Structure*; University of Göttingen: Göttingen, Germany, 1997. (c) Sheldrick, G. M. *Acta Crystallogr.* **2008**, *A64*, 112−122.
(61) Frisch, M. J.; Trucks, G. W.; Schlegel, H. B.; Scuseria, G. E.; Robb, M. A.; Cheeseman, J. R.; Montgomery, J. A., Jr.; Vreven, T.; Kudin, K. N.; Burant, J. C.; Millam, J. M.; Iyengar, S. S.; Omasi, J.; Barone, V.; Mennucci, B.; Cossi, M.; Scalmani, G.; Rega, N.; Petersson, G. A.; Nakatsuji, H.; Hada, M.; Ehara, M.; Toyota, K.; Fukuda, R.; Hasegawa, J.; Ishida, M.; Nakajima, T.; Honda, Y.; Kitao, O.; Nakai, H.; Klene, M.; Li, X.; Knox, J. E.; Hratchian, H. P.; Cross, J. B.; Adamo, C.; Jaramillo, J.; Gomperts, R.; Stratmann, R. E.; Yazyev, O.; Austin, A. J.; Cammi, R.; Pomelli, C.; Ochterski, J. W.; Ayala, P. Y.; Orokuma, K.; Voth, G. A.; Salvador, P.; Dannenberg, J. J.; Zakrzewski, V. G.; Dapprich, S.; Daniels, A. D.; Strain, M. C.; Farkas, O.; Malick, D. K.; Rabuck, A. D.; Raghavachari, K.; Foresman, J. B.; Ortiz, J. V.; Cui, Q.; Baboul, A. G.; Clifford, S.; Cioslowski, J.; Stefanov, B. B.; Liu, G.; Liashenko, A.; Piskorz, P.; Komaromi, I.; Martin, R. L.; Fox, D. J.; Keith, T.; Al-Laham, M. A.; Peng, C. Y.; Nanayakkara, A.; Challacombe, M.; Gill, P. M. W. ; Johnson, B.; Chen, W.; Wong, M. W.; Gonzalez, C.; Pople, J. A. *Gaussian 03*, revision B.03; Gaussian, Inc.: Pittsburgh, PA, 2003.
(62) Bernadou, J.; Prativiel, G.; Bennis, F.; Girardet, M.; Meunier, B. *Biochemistry* **1989**, *28*, 7268−7275.
(63) Povirk, L. F.; Wubker, W.; Kohnlein, W.; Hutchinson, F. *Nucleic Acids Res.* **1977**, *4*, 3573.
(64) Freifelder, D.; Trumbo, B. *Biopolymers* **1969**, *7*, 681.
(65) Quiming, N. S.; Vergel, R. B.; Nicolas, M. G.; Villanueva, J. A. *J. Health Sci.* **2005**, *51*, 8−15.
(66) Laemmli, U. K. *Nature* **1970**, *227*, 680−685.
(67) Blagosklonny, M.; El-Diery, W. S. *Int. J. Cancer.* **1996**, *67*, 386−392.
(68) Kasibhatla, G. P. A. H.; Finucane, D.; Brunner, T.; Wetzel, E. B; Green, D. R. Protocol: Staining of suspension cells with Hoechst 33258 to detect apoptosis. *Cell: A Laboratory Manual Culture and Biochemical Analysis of Cells*; CSHL Press: USA, 1998; vol. *1*, p 15.5.
(69) Sihn, C. R.; Suh, E. J.; Lee, K. H.; Kim, T. Y.; Kim, S. H. *Cancer Lett.* **2003**, *201*, 203−210.
(70) Heffeter, P.; Jakupec, M. A.; Körner, W.; Wild, S.; Von Keyserlingk, N. G.; Elbling, L.; Zorbas, H.; Koryneuska, A.; Knasmüller, S.; Sutterlüty, H.; Micksche, M.; Keppler, B. K.; Berger, W. *Biochem. Pharmacol.* **2006**, *71*, 426.
(71) (a) Filomeni, V.; Cerchiaro, G.; Da Costa Ferreira, A. M.; Martino, A. D.; Pedersen, J. Z.; Rotilio, G.; Ciriolo, M. R. *J. Biol. Chem.* **2007**, *282*, 12010−12021. (b) Guo, W.; Ye, S.; Cao, N.; Huang, J.; Gao, J.; Chen, Q. *Exp. Toxicol. Pathol.* **2010**, *62*, 577−582.
(72) (a) Sakaguchi, U.; Addison, A. W. *J.C.S. Dalton* **1979**, 600. (b) Palaniandavar, M.; Somasundaram, I.; Lakshminarayanan, M.; Manohar, H. *Dalton Trans.* **1996**, 1333−1340. (c) Huheey, J. E.; Keiter, E. A.; Keiter, R. L.; Medhu, O. K. *Inorganic Chemistry, Principles of Structure and Reactivity*; Pearson Education: Upper Saddle River, NJ, 2006, 425−426.
(73) (a) Peisach, J.; Blumberg, W. E. *Arch. Biochem. Biophys.* **1974**, *165*, 691−708. (b) Murali, M.; Palaniandavar, M.; Pandiyan, T. *Inorg. Chim. Acta* **1994**, *224*, 19.
(74) (a) Addison, A. W.; Rao, T. N.; Reedijk, J.; Rijn, J. V.; Verschoor, G. C. *J. Chem. Soc., Dalton Trans.* **1984**, 1349−1356. (b) Murphy, G.; Nagle, P.; Murphy, B.; Hathway, B. *Dalton Trans.* **1997**, 2645−2652.
(75) Murphy, G.; Murphy, C.; Murphy, B.; Hathway, B. *Dalton Trans.* **1997**, 2653−2660.
(76) Nagle, P.; O'Sullivan, E.; Hathway, B. *J. Chem. Soc., Dalton Trans.* **1990**, 3399−3406.
(77) Tamil Selvi, P.; Murali, M.; Palaniandavar, M.; Kockerling, M.; Henkel, G. *Inorg. Chim. Acta B* **2002**, *340*, 139−146.
(78) (a) Palaniandavar, M.; Pandiyan, T.; Lakshminarayanan, M.; Manohar, H. *J. Chem. Soc., Dalton Trans.* **1995**, *3*, 455. (b) Pijus, K.; Sasmal, Saha, S.; Majumdar, R.; Dighe, R. R.; Chakravarty, A. R. *Inorg. Chem.* **2010**, *49*, 849−859. (c) Liu, J.; Song, Z.; Wang, L.; Zhuang, J.; You, X.; Huang, X. *Transition Met. Chem.* **1999**, *24*, 499.
(79) (a) Chena, Z.; Wang, X.; Li, Y.; Guo, Z. *Inorg. Chem. Commun.* **2008**, *11*, 1392−1396. (b) Arjmand, F.; Chauhan, M. *Helv. Chim. Acta* **2005**, *88*, 2413.
(80) Ramakrishnan, S.; Palaniandavar, M. *Dalton Trans.* **2008**, 3866.
(81) Maheswari, P. U.; Rajendiran, V.; Evans, H. S.; Palaniandavar, M. *Inorg. Chem.* **2006**, *45*, 37.
(82) Ramakrishnan, S.; Palaniandavar, M. *J. Chem. Sci.* **2005**, *117*, 179.
(83) Maheswari, P. U.; Rajendiran, V.; Parthasarathi, R.; Subramanian, V.; Palaniandavar, M. *Bull. Chem. Soc. Jpn.* **2005**, *78*, 835.
(84) Maheswari, P. U.; Palaniandavar, M. *Inorg. Chim. Acta* **2004**, *357*, 901.
(85) Morgan, A. R; Lee, J. S.; Pulleyblank, D. E.; Evans, D. H. *Nucleic Acid Res.* **1979**, *7*, 547.
(86) (a) Ivanov, V. I.; Minchenkova, L. E.; Schyolkina, A. K.; Polytayer, A. I. *Biopolymers* **1973**, *12*, 89. (b) Pezzano, H.; Podo, F. *Chem. Rev* **1980**, *80*, 392. (c) Saha, B.; Islam, Md. M.; Paul, S.; Samanta, S.; Ray, S.; Santra, C. R.; Choudhury, S. R.; Dey, B.; Das, A.; Ghosh, S.; Mukhopadhyay, S.; Kumar, G. S.; Karmakar, P. *J. Phys. Chem. B* **2010**, *114*, 5851−5861. (d) Mahadevan, S.; Palaniandavar, M. *Inorg. Chem.* **1998**, *37*, 3927.
(87) Collins, J. G.; Shields, T. P.; Barton, J. K. *J. Am. Chem. Soc.* **1994**, *116*, 9840.

(88) Liu, J. G.; Zhang, Q. L.; Ji, L. N. *Transition Met. Chem.* **2001**, *26*, 733.
(89) Povirk, L. F.; Houlgrave, C. W. *Biochemistry* **1988**, *27*, 3850.
(90) Drak, J.; Iwasawa, N.; Danishefsky, S.; Crothers, D. M. *Proc. Natl. Acad. Sci. U.S.A.* **1991**, *88*, 7464.
(91) Peters, T. *Adv. Protein Chem.* **1985**, *37*, 161−245.
(92) (a) Halfman, C. J.; Nishida, T. *Biochim. Biophys. Acta* **1971**, *243*, 284−293. (b) Halfman, C. J.; Nishida, T. *Biochim. Biophys. Acta* **1971**, *243*, 294−303.
(93) Lakowicz, J. R. *Principles of Fluorescence Spectroscopy*, 2nd ed.; Plenum Press: New York, 1999.
(94) Kumar, C. V.; Buranaprapuk, A.; Sze, H. C.; Jockusch, S.; Turro, N. J. *Proc. Natl. Acad. Sci. U. S. A.* **2002**, *99*, 5810−5815.
(95) (a) de Oliveira, M. C. B.; Scarpellini, M.; Neves, A.; Terenzi, H.; Bortoluzzi, A. J.; Szpoganics, B.; Greatti, A.; Mangrich, A. S.; de Souza, E. M.; Fernandez, P. M.; Soares, M. R. *Inorg. Chem.* **2005**, *44*, 921. (b) Messori, L.; Orioli, P.; Vullo, D.; Alessio, E.; Lengo, E. *Eur. J. Biochem.* **2000**, *267*, 1206−1213.
(96) Ghobrial, I. M.; Witzig, T. E.; Adjei, A. A. *Ca-Cancer J. Clin.* **2005**, *55*, 178.
(97) Alapetite, C.; Wachter, T.; Sage, E.; Moustacchi, E. *Int. J. Radiat. Biol.* **1996**, *69*, 359.
(98) Liu, L.; Zhang, H.; Meng, X.; Yin, J.; Li, D.; Liu, C. *Biomaterials* **2010**, *31*, 1380.